THESIS

LAND OF 10,000 PIXELS: APPLICATIONS OF REMOTE SENSING & GEOSPATIAL DATA TO IMPROVE FOREST MANAGEMENT IN NORTHERN MINNESOTA, USA

Submitted by

Peder Engelstad

Department of Ecosystem Science and Sustainability

In partial fulfillment of the requirements

For the Degree of Master of Science

Colorado State University

Fort Collins, Colorado

Summer 2018

Master's Committee:

Advisor: Michael Falkowski

Michael Lefsky
Mark Paschke

ABSTRACT

LAND OF 10,000 PIXELS: APPLICATIONS OF REMOTE SENSING & GEOSPATIAL DATA TO IMPROVE FOREST MANAGEMENT IN NORTHERN MINNESOTA, USA

The use of remote sensing and geospatial data has become commonplace in a wide variety of ecological applications. However, the utility of these applications is often limited by field sampling design or the constraints on spatial resolution inherent in remote sensing technology. Because land managers require map products that more accurately reflect habitat composition at local, operational levels there is a need to overcome these limitations and improve upon currently available data products. This study addresses this need through two unique applications demonstrating the ability of remote sensing to enhance operational forest management at local scales.

In the first chapter, remote sensing products were evaluated to improve upon regional estimates of the spatial configuration, extent, and distribution of black ash from forest inventory and analysis (FIA) survey data. To do this, spectral and topographic indices, as well as ancillary geospatial data were combined with FIA survey information in a non-parametric modeling framework to predict the presence and absence of black ash dominated stands in northern Minnesota, USA. The final model produced low error rates (Overall: 14.5%, Presence: 14.3%, Absence: 14.6%; AUC: 0.92) and was strongly informed by an optimized set of predictors related to soil saturation and seasonal growth patterns. The model allowed the production of accurate, fine-scale presence/absence maps of black ash stand dominance that can ultimately be used in support of invasive species risk management.

In the second chapter, metrics from low-density LiDAR were evaluated for improving upon estimates of forest canopy attributes traditionally accessed through the LANDFIRE program. To do this, LiDAR metrics were combined with a Landsat time-series derived canopy cover layer in random forest *k*-nearest neighbor imputation approach to estimate canopy bulk density, two measures of canopy base height, and stand age across the Boundary Waters Canoe Area in northern Minnesota, USA. These models produced strong relationships between the estimates of canopy fuel attributes and field-based data for stand age (R^2 = 0.82, RMSE = 10.12 years), crown fuel base height (R^2 = 0.79, RMSE = 1.10 m.), live crown base height (R^2 = 0.71, RMSE 1.60 m.), and canopy bulk density (R^2 = 0.58, RMSE 0.09 kg/m^3). An additional standard randomForest model of canopy height was less successful (R^2 = 0.33, RMSE 2.08 m). The map products generated from these models improve upon the accuracy of national available canopy fuel products and provide local forest managers with cost-efficient and operationally ready data required to simulate fire behavior and support management efforts.

ACKNOWLEDGEMENTS

I would first like to acknowledge my advisor, Dr. Michael Falkowski for providing this fantastic opportunity to learn what it really means to call myself a scientist. I truly appreciate all the support, guidance, and patience Dr. Falkowski has afforded me over the last two years. I also acknowledge the other members of my committee, Dr. Michael Lefsky and Dr. Mark Paschke, for their expertise and thoughtful contributions to my research.

Family, friends, professors, and colleagues were inexhaustible sources of knowledge, expertise, and enlightening conversations that all helped me find my way to the completion of this thesis. I am especially grateful for help from Steve Filippelli, as well as Grant Domke, Brian Woodward, Tony Vorster, Magda Garbowski, Melinda Laituri, Linda Nagel, Paul Evangelista, Wilfred Previant, Aaron Poznanovic, Jacob Muller, Sarah Carroll, Amanda West, Peter Wolter, Scott and Laura Engelstad, and so many others.

Finally, none of this would have been possible without the infinite patience and calming influence of my lovely wife, Andrea Engelstad. Thank you for encouraging me when I doubted myself, listening to my nerdy excitement, and for taking this journey with me.

TABLE OF CONTENTS

LIST OF TABLES

LIST OF FIGURES

CHAPTER 1: MAPPING BLACK ASH DOMINATED STANDS USING FOREST INVENTORY DATA AND REMOTE SENSING

Introduction

The introduced emerald ash borer (EAB; *Argilus planipennis* Fairemaire) has been a persistent disturbance on ash forests in the United States since 2002 and is advancing into northern portions of the Upper Great Lakes states. Of particular concern is the impact EAB will have on the ecological and hydrological functioning of wetlands dominated by black ash (*Fraxinus nigra*). In preparation, forest managers need reliable and complete maps of the spatial configuration, extent, and distribution of black ash. Traditionally, the Forest Inventory and Analysis (FIA) program has provided rigorous measures of tree species presence at large spatial extents (e.g., species range maps) but such data are limited with regard to providing estimates at smaller management unit extents (e.g., stands). Fortunately, remotely sensed data can be leveraged to spatially extend forest survey information collected by FIA to predict forest attributes at extents smaller than the FIA sampling grid. To accomplish this, spectral and topographic indices, as well as ancillary geospatial data layers were integrated with FIA data in a non-parametric modelling framework (randomForest) to spatially predict and map black ash stand dominance in northern Minnesota, USA. Model selection techniques were employed to optimize the ecological interpretability and parsimony of the resulting prediction model. Additionally, during model development, a majority-class downsampling approach was used to minimize the negative effects of imbalanced sampling. This resulted in a final model that produced low error rates (Overall error: 14.5%, Presence error: 14.3%, Absence error: 14.6%; AUC: 0.92) and was strongly informed by an optimized set of predictors related to soil saturation

and unique phenological patterns of black ash. Results from this study provide forest managers with accurate, fine-scale presence/absence maps of black ash stand dominance that could ultimately be used to support EAB risk and vulnerability assessments across large spatial extents.

Background

A variety of exotic flora, fauna, and pathogens induce ecological changes to forested ecosystems worldwide, ultimately disrupting nutrient cycling, productivity, and wildlife habitat, among others (Lovett et al., 2016). In the short term, exotic species can alter forest floor environments and create canopy gaps, while long-term changes may affect entire forest successional trajectories (Gandhi and Herms, 2010). One such exotic species is the introduced emerald ash borer (EAB; *Agrilus planipennis* Fairmaire), a wood-boring beetle that was first discovered in southeast Michigan in 2002. EAB attacks all ash trees regardless of health and size (Herms and McCullough, 2014), killing hosts in as little as two years (Knight et al., 2013). Due to widespread municipal planting of ash trees, much of the research on EAB impact and mitigation strategies has been restricted to urban environments (i.e. Crook et al., 2008; Poland and McCullough, 2006; Kovacs et al., 2010). However, EAB range expansion and the associated threat to non-urban ash forests is expected to grow due to factors such as illegal firewood transportation (BenDor et al., 2006) and warming climate scenarios (Liang and Fei, 2014).

One ash species of particular concern is black ash (*Fraxinus nigra*), a slow-growing hardwood tree often found in relatively pure stands on poorly drained soils. The native range of black ash spans from western Newfoundland to southeastern Manitoba, Canada south to Iowa and Ohio, and east to northern Virginia, USA (Wright and Rauscher 1990). Black ash is

considered to function as a foundational tree species, and thereby strongly regulates ecosystem processes (Ellison et al., 2005). Rapid stand mortality of black ash from EAB attack is expected to have significant impacts on ecosystem structure and function (Slesak et al., 2014). Indeed, dramatic disruptions are anticipated in native plant communities and wildlife food webs (DeSantis et al., 2013; Youngquist et al., 2017), biogeochemical processes (Flower et al., 2013) and resistance to invasion by exotic flora (Kenis et al., 2009; Klooster et al., 2012). Additionally, the reduction in evapotranspiration accompanying the loss of black ash may permanently shift vegetation types in these communities from forests to marsh-like ecosystems, and may ultimately increase flood risk (Telander et al., 2015). The loss of black ash also poses a distinct threat to multiple indigenous groups' cultural practices in the northern Great Lakes states by reducing wood sources traditionally used for basketmaking (Costanza et al., 2017; Willow, 2011).

To help address and minimize these risks, forest managers need reliable and complete maps depicting the spatial configuration, extent, and distribution of black ash. Large-area estimates of tree species distributions can be generated from systematic forest inventory data collected via national forest inventory surveys; however, such data do not provide specific predictions of species occurrence at spatial extents smaller than that of the systematic sampling grid (McRoberts and Tomppo, 2007). In the United States, the U.S. Forest Service's Forest Inventory and Analysis program (FIA) provides forest inventory information through annual surveys via a variety of on-the-ground field measurements (Bechtold and Patterson, 2005). The sampling methodology of FIA ensures robust estimates at county, state, regional, and national levels. However, smaller spatial units (e.g., forest district management units, stands, etc.) often contain an insufficient number of plots to generate precise local estimates of forest attributes and descriptions of their spatial characteristics (Goerndt et al., 2013).

Fortunately, this problem of small area estimation (SAE) has been successfully addressed in previous studies by combining FIA data with predictors derived from a variety of remote sensing sources to generate predictions of forest attributes. For example, multispectral data from passive optical sensors have been leveraged to estimate basal area (McRoberts et al., 2007), forest disturbance (Shroeder et al., 2014), stand density (McRoberts, 2009), successional stage (Liu et al., 2008), and canopy cover (Coulston et al., 2012), among others. Active remote sensing techniques, such as light ranging and detection (LiDAR), have been used in conjunction with data from FIA to model biomass (Andersen et al., 2009), stand volume (Sheridan et al., 2014), and fire effects (Alonzo et al., 2017).

Species occurrence data from FIA has also been used to classify forest types, and is often combined with multiple remote sensing or geospatial resources that help define the biotic and abiotic niche of target species. For example, Evans and Cushman (2009) used topographic indices and Landsat data to estimate occupancy of four conifer species in northern Idaho. In Maine, Dunckel et al (2015) mapped eastern Hemlock occurrence by combining climate, soil, and topographic indices with Landsat data. To map the extent of eastern hemlock in eastern Kentucky, Clark et al (2012) employed predictors derived from topography, soils, and climate data. In Utah, Zimmerman et al (2007) compared the effectiveness of topographic and bioclimatic predictors to vegetation indices from Landsat for species-level classification of over a dozen tree species. Finally, Franco-Lopez et al (2001) generated maps of tree cover types in northeastern Minnesota from Landsat and ancillary geospatial data.

The objective of this study was to combine spectral and topographic indices, and ancillary geospatial layers with data from FIA field surveys to classify black ash dominated stands across a diverse forest landscape in northern Minnesota, USA. Specifically, this study

focused on predictors potentially indicative of soil moisture and phenology in an attempt to more fully describe the ecological niche of black ash. In the development of this approach, a model selection procedure was used to evaluate the most important predictors for classifying black ash stands and generated a highly accurate, parsimonious model that accounted for class imbalance. Model performance was evaluated via traditional accuracy assessment statistics and by conditional density plots to determine if the model produced ecologically meaningful results. Furthermore, a spatial assessment of classification stability was performed to explore the potential sources of error when classifying stand dominance across a diverse array of forest conditions.

Methods

Study area

The study area is defined by the extent of a Landsat scene (WRS-2 Path 28/Row 27) in northern Minnesota, USA (Figure 1.1). The area (~36,000 km^2) sits on the transition zone between boreal and mixed forest types resulting in a diverse, heterogeneous mix of hardwood and conifer species, as well as conifer bogs and hardwood swamps. Historical climate records (1981-2010) indicate an average rainfall of 54 to 81 cm (MN DNR, 2017) and elevation ranges from ~ 350 to 600 m above sea level. The study area contains a mix of public and private lands, including the entirety of the Chippewa National Forest. The study area was selected due to the availability of statewide LiDAR products in Minnesota and cloud-free Landsat imagery coterminous with the most recent year of publicly accessible FIA data. Placing the study in the

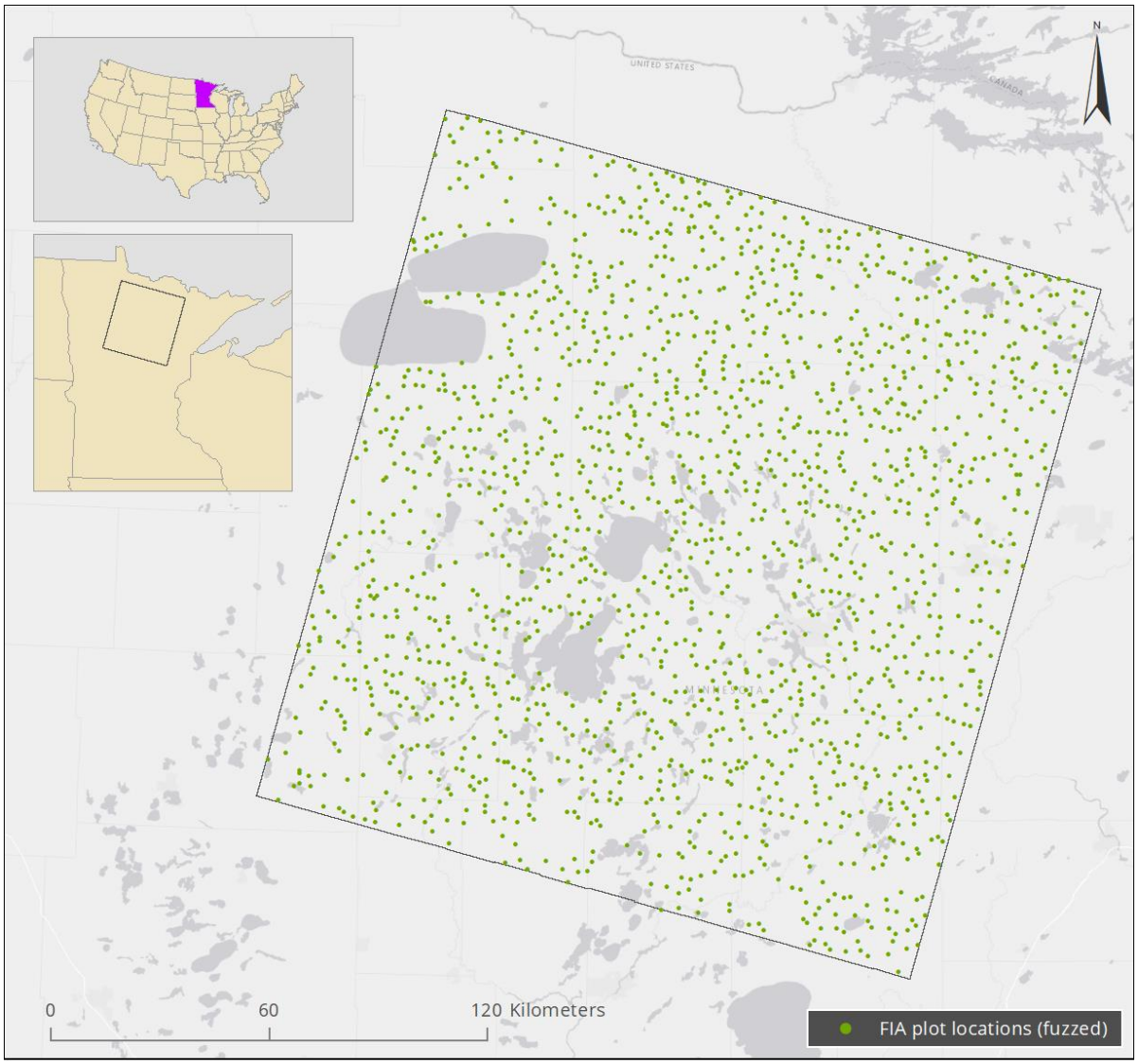

Figure 1.1. Spatial extent of the study area in northern Minnesota, USA. All Forest Inventory and Analysis plots (n=1765) evaluated during model development are shown for the 2011-2015 data collection cycle.

forests of northern Minnesota is also relevant due to their proximity to ongoing EAB outbreaks as well as the predicted northward shifts in EAB range (Liang and Fei, 2014).

Data collection

Field data used in this study consisted of FIA plots measured during a single inventory cycle between 2011 and 2015. The sampling design of FIA consists of long-term survey sites systematically stratified across public and private lands, with each site consisting of four 0.02 ha ($1/24^{th}$ acre) fixed radius subplots (Figure 1.2). The large number of forest attributes collected at each site generally fall in to two categories: site description and direct measurement. Site descriptions include observations of forest type, condition (forest or non-forest), and disturbance. Measurements recorded at the individual tree level include standard forestry metrics such as diameter at breast height (DBH), tree height, and tree age.

To quantify stand dominance, basal area was calculated for each species using DBH (Equation 1). Basal area is understood as a correlate of stand density and has been successfully used in previous remote sensing studies of forest species occurrence (Duveneck et al., 2015; Goerndt et al., 2013; Martin et al., 1998; Moisen et al., 2006; Ohmann and Gregory, 2002). Total basal area for the plot was determined by scaling to the hectare-level using an expansion factor (ω) listed in the FIA database (Equation 2) for living trees >= 12.7 cm DBH. The relative dominance for each species in the plot was calculated as the total basal area by species divided by the total plot basal area.

Researchers studying the impacts of EAB on black ash systems have not yet established a consensus on the percentage of stand mortality necessary to cause significant ecohydrological effects (Kolka, et al., 2018). Therefore, to explore one measure of stand dominance, plots with a

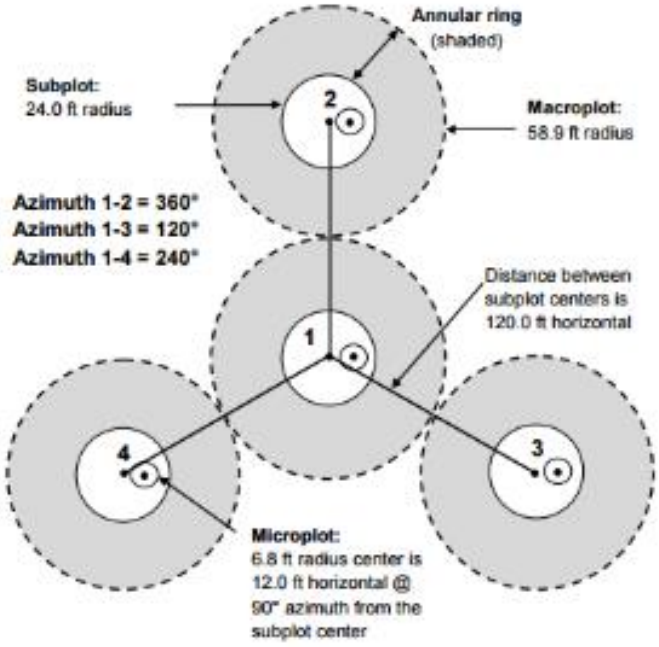

Figure 1.2. The national standard phase 2 plot design for the Forest Inventory and Analysis program administered by the U.S. Forest Service.

simple majority (>= 50% of total plot basal area) of black ash were assigned binary value of presence (1). Plots where black ash accounted for less than 50% of total basal area were assigned as absence (0). From an initial 1,765 field plots available during the inventory cycle, 923 remained after retaining only undisturbed, single land cover condition, forested plots. The application of the stand dominance threshold resulted in training data that included 874 absence and 49 presence points.

$$BA\ (m^2) = \left(\frac{\pi}{4 * 10000}\right) * DBH^2$$

(Equation 1)

$$BA/hectare = \sum_{i=1}^{n} BA_i\ \omega_i$$

(Equation 2)

Remote sensing data

The use of active and passive remote sensing data is common in ecological research. Specific to species-level classification, these data can potentially describe the biophysical characteristics of the target species' environmental niche and growth patterns. For this study, a LiDAR-derived digital terrain model (MNGeo, 2017) was used to derive 20 m resolution topographic indices that describe a variety of soil attributes (Table 1.1). To characterize the wet soils typical of dense black ash stands, indices were chosen that reflect soil moisture potential (Compound Topographic Index), solar temperature effects (Heat Load Index), and water-holding capacity (Integrated Moisture Index) in addition to standard topography metrics such as elevation, slope, and aspect.

While LiDAR data are extremely useful for characterizing topography and forest structure, they are generally of limited use for discriminating between different species due to limited spectral and temporal information (Fassnacht, et al., 2016). Fortunately, multispectral satellite sensors collect data with higher spectral and temporal resolution, facilitating species differentiation and seasonal averaging. In this study, Landsat 8 single-date (9/13/2015), cloud-free, surface-reflectance vegetation indices were acquired from USGS (Table 1.1) at a 30 m resolution. Additionally, Google Earth Engine (https://earthengine.google.com) was used to generate minimum, maximum, median, and differenced values for normalized burn ratio (NBR), normalized difference vegetation index (NDVI) and normalized difference moisture index (NDMI) at a 30 m resolution (Table 1.1) within a date range long enough to capture the growth cycles of multiple forest species (April 1st to October 31st, 2015). The goal of including

Table 1.1. The 44 candidate predictor variables evaluated during development of the randomForest classification of black ash stand dominance in northern Minnesota. Variables included in the final model are indicated in bold.

Variable	Description
CTI	Compound Topographic Index
CURVE	Slope Curvature
doy_EVI	Single-Date Enhanced Vegetation Index
doy_IFZ	Single-Date Integrated Forest Z-Score
doy_MSAVI	Single-Date Modified Soil-Adjusted Vegetation Index
doy_NBR	Single-Date Normalized Burn Ratio
doy_NDMI	Single-Date Normalized Difference Moisture Index
doy_NDVI	Single-Date Normalized Difference Vegetation Index
doy_SAVI	Single-Date Soil-Adjusted Vegetation Index
dNBR	Summer Minus Fall Median Differenced Normalized Burn Ratio
dNDMI	Summer Minus Fall Median Normalized Difference Moisture Index
dNDVI	Summer Minus Fall Median Normalized Difference Vegetation Index
ELEV	Elevation (meters)
fall_NBR	Median Normalized Burn Ratio (Sept-Oct)
fall_NDMI	Median Normalized Difference Moisture Index (Sept-Oct)
fall_NDVI	Median Normalized Difference Vegetation Index (Sept-Oct)
grow_NBR	Median Normalized Burn Ratio (Apr-Oct)
grow_NDMI	Median Normalized Difference Moisture Index (Apr-Oct)
grow_NDVI	Median Normalized Difference Vegetation Index (Apr-Oct)
HLI	Heat Load Index
IMI	Integrated Moisture Index
JSmax_NBR	Maximum Normalized Burn Ratio (June-Sept)
JSmax_NDMI	Maximum Normalized Difference Moisture Index (June-Sept)
JSmax_NDVI	Maximum Normalized Difference Vegetation Index (June-Sept)
JSmin_NBR	Minimum Normalized Burn Ratio (June-Sept)
JSmin_NDMI	Minimum Normalized Difference Moisture Index (June-Sept)
JSmin_NDVI	Minimum Normalized Difference Vegetation Index (June-Sept)
JSmed_NBR	Median Normalized Burn Ratio (June-Sept)
JSmed_NDMI	Median Normalized Difference Moisture Index (June-Sept)
JSmed_NDVI	Median Normalized Difference Vegetation Index (June-Sept)
ROUGH	Terrain Roughness
SOILS_DI	SSURGO Soil Drainage Index
SOILS_PI	SSURGO Soil Productivity Index
summ_NBR	Summer Normalized Burn Ratio (Jul-Aug)
summ_NDMI	Summer Normalized Difference Moisture Index (Jul-Aug)
summ_NDVI	Summer Normalized Difference Vegetation Index (Jul-Aug)
TCAP_A	Tasseled Cap Angle
TCAP_B	Tasseled Cap Brightness
TCAP_D	Tasseled Cap Distance
TCAP_DI	Tasseled Cap Disturbance Index
TCAP_G	Tasseled Cap Greenness
TCAP_W	Tasseled Cap Wetness
TRASP	Transformed Aspect
WETLAND	National Wetlands Inventory Category

seasonally descriptive predictors was to differentiate the phenological signature of black ash (defined by smaller annual leaf area growth and a restricted number of growing days) from co-occurring deciduous tree species.

Ancillary geospatial data

To further capture the abiotic niche of black ash, geospatial data were acquired from the National Wetlands Inventory (NWI), which uses manual interpretation of aerial imagery to produce a detailed hierarchical classification of wetland habitat types (Dahl et al., 2009). Following previous research establishing forest wetlands as the primary habitat of black ash (Wright and Rauscher, 1990), NWI data was used to develop a categorical predictor that would discriminate forested from non-forested wetlands. Soil indices were also acquired from the Soil Survey Geographic Database (SSURGO; Soil Survey Staff 2015), which provide useful measures of soil inundation and nutrient quality. First, a drainage index, designed to measure long-term soil wetness, was used to relate black ash with heavily inundated soils. Second, the incorporation of a productivity index, interpreted from soil taxonomy, provided a measure related to the nutrient content of soils where black ash is found.

Predictor variable development

FIA plots are located on their own grid system irrespective of any predictor variable alignment used in this study. To address this, a 3 x 3 focal mean moving window was applied to continuous predictor variables, resolving the spatial incongruity of the larger FIA plot design (~ 90 x 90-m) relative to that of the predictors (30 x 30 m). This method has been previously used to partially alleviate co-registration errors between remotely sensed predictors and FIA data

incorporating all four subplots (Dunckel et al., 2017; Moisen et al., 2006; Nelson et al., 2009; Powell et al., 2010). However, as noted by McRoberts (2009), one consequence of using all four subplots is a potential reduction in training data size, if filtering out non-homogeneous forest cover conditions.

Model development

A presence and absence classification model of black ash stand dominance was developed using the randomForest algorithm (RF; Breiman, 2001) as implemented in the 'randomForest' package (Liaw and Wiener, 2002) of the R statistical software (R Core Development Team, 2017). The RF model was run with 4,000 bootstrapped replicates (*ntrees*), with replacement, to stabilize error rates, variable importance, and variable interaction (Evans and Cushman, 2009). Although RF is considered robust to collinearity (Cutler et al., 2007), a model selection procedure was used to reduce the number of redundant predictors while retaining ecological interpretability (Falkowski et al., 2009). Prior to model selection, a Gram-Schmidt QR decomposition procedure, which is in the R 'rfUtilities' package (Evans et al., 2011), was used to identify and remove multicollinear predictor variables. To further optimize model parsimony, the 'model selection' function, also available in 'rfUtilities', was implemented. This function iterates through and evaluates potential models (i.e., suites of potential predictor variables) by assessing possible variable combinations, and comparing them based on a model improvement ratio (MIR) statistic (Murphy et al., 2010) that measures the difference in percentage change in overall out-of-bag error.

Addressing class imbalance

In machine learning, class size imbalance remains a regular source of bias, often resulting in the majority class being favored over the minority class (He and Garcia, 2009; Japkowicz and Stephen, 2002). Specific to RF, the iterative bootstrap sample of training data often lacks a representative sample from the minority class. To address this, downsampling the majority class has previously been shown to be more effective in overcoming majority class bias when compared to oversampling and weighted class methods (Chen et al., 2004; Drummond and Holte, 2003). In this study, the majority class (i.e., absence) was downsampled to match the size of the minority (i.e., presence) class (n = 49) for each bootstrap sample to minimize bias from class imbalance.

Accuracy assessment and model evaluation

Classification accuracy was measured based on internal error estimates from out-of-bag samples generated by the RF model. Overall accuracy as well as errors of omission and commission were calculated to explore the accuracy of presence and absence classes produced by the model. The model was also assessed using the Area Under the Curve (AUC) statistic, generated from a Receiver Operator Curve (ROC) comparing the true positive rate (sensitivity) against the true negative rate (specificity). After this, the model was applied to the geospatial datasets to produce a binary classification of presence and absence of black ash dominance across the study area. Model uncertainty was also assessed through visual inspection of a maximum value class probability map to summarize the uncertainty of the binary classification predictions. Finally, conditional density plots, which display the probability of class occurrence

across the range of values for a single predictor, were examined for the most important predictors (identified by RF) to verify the production of an ecologically reasonable model.

Results

Model selection

The Gram-Schmidt QR decomposition procedure identified and removed 33 multicollinear predictors. The secondary model selection function (MIR statistic) did not identify further model parsimony optimizations for the binary classification of black ash dominated stands. This left twelve predictor variables that were used to develop the RF classification model: Compound Topographic Index (CTI), Summer-Fall Differenced NBR, June-September Minimum NDMI, Tasseled Cap (TC) Brightness, TC Greenness, TC Wetness, TC Disturbance Index, Single-Date NBR, Single-Date Enhanced Vegetation Index (EVI), Single-Date NDMI, and NWI wetland class (Table 1.1).

Classification accuracy and variable importance

The overall accuracy of the final model was 85.5% and the AUC value was 0.92. Individual class and omission and commission errors were low (Table 1.2). However, some confusion did occur in the form of false positives, resulting in a 24.7% error rate. The investigation of variable importance (Figure 1.3) indicated CTI as the most important, followed closely by TC Disturbance Index (TCAP DI), Summer-Fall Differenced NBR (dNBR), and June-September Minimum NDMI (JSminNDMI).

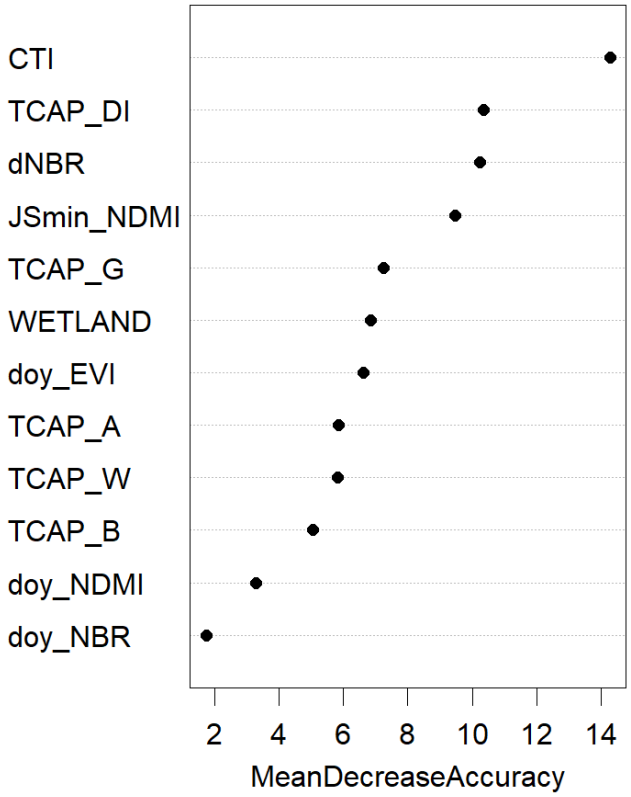

Figure 1.3. Plot of variable importance values for the predictors used in the final randomForest model of black ash dominated stand presence/absence. 'MeanDecreaseAccuracy' measures the amount of accuracy lost with the removal of the individual variable.

Table 1.2. Classification accuracy statistics for the randomForest model of presence and absence of black ash stand dominance.

Class	**Omission Error (Producer)**	**Commission Error (User)**	**Class Accuracy**
Presence	4.7	14.3	85.7
Absence	24.7	14.6	85.4
Overall accuracy	85.5%		

Model evaluation

The class probability map (Figure 1.4), illustrates the prediction stability of both presences and absences. The majority of the study area (~60%) had a classification stability of over 80%. In contrast, approximately 14% of the study area was represented by stability under 60%. Initial visual interpretation of low stability pixels indicated high instability occurrence in areas of forest disturbance (i.e. harvest) during the years of data collection (Figure 1.5). Conditional density plots (Figure 1.6) were examined to verify that the model produced ecologically meaningful results. The plots represent the relationship between the probability of presence or absence classes and the four most important predictors. For the presence class, an increasing likelihood of presence is generally associated with increasing values of CTI, TCAP DI, and dNBR. The inverse is true for JSminNDMI, where the likelihood of presence quickly decreases for values above ~ 0.25.

Discussion

The RF model developed in this study effectively classified the presence and absence of black ash dominated stands while addressing potential class imbalance bias. The maps produced are operationally ready estimates of the spatial configuration, distribution, and extent of black ash in northern Minnesota, USA. These results successfully overcome the SAE limitations inherent in the FIA sampling methodology and represent local estimates of a species at risk of potential habitat loss due to EAB.

The accuracies presented here are similar to, or improve upon, the limited research generating species level classifications of black ash from remotely sensed data. For example,

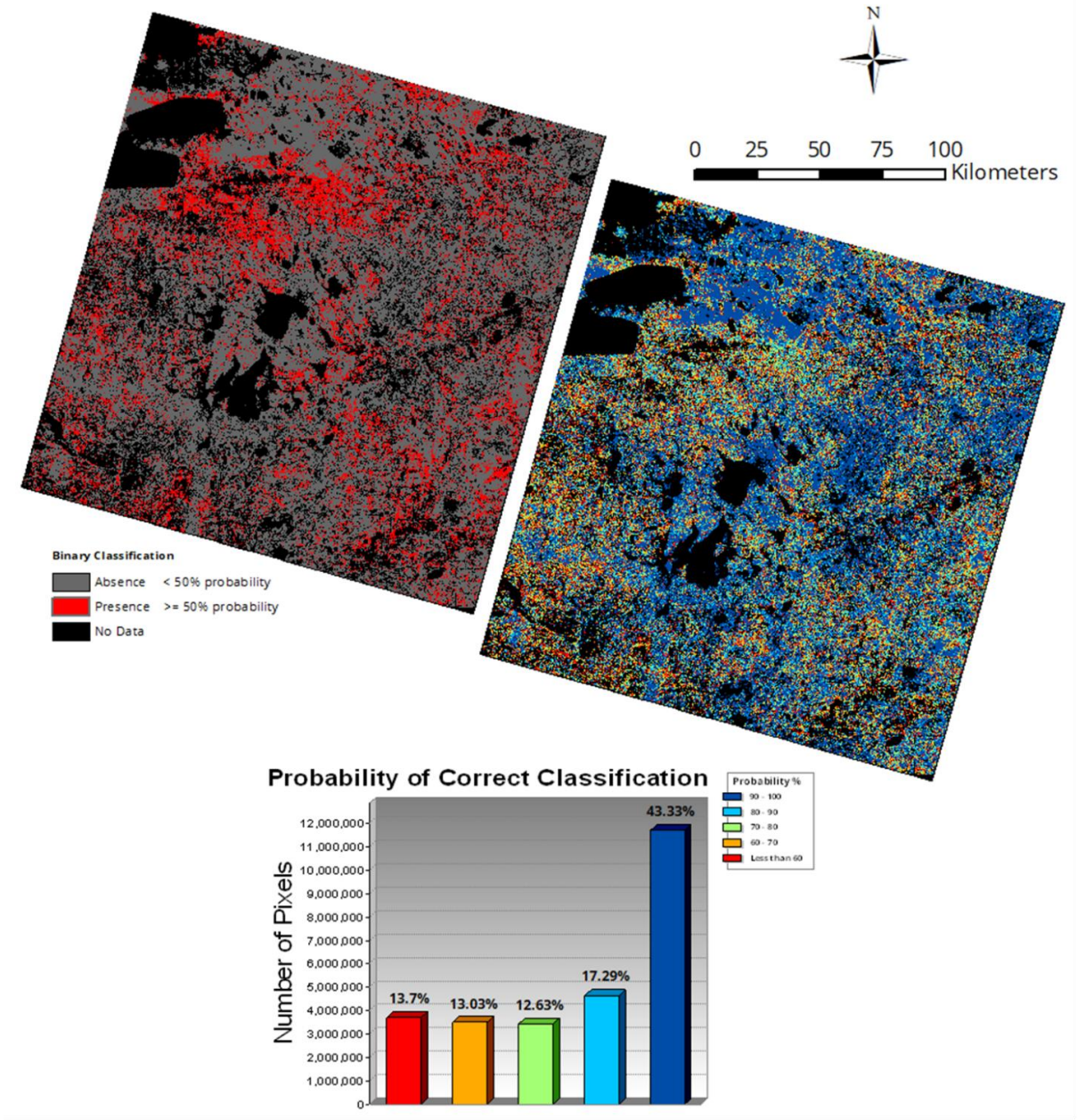

Figure 1.4. Binary classification, maximum probability (classification stability) map, and output summary statistics produced by the randomForest model of black ash stand dominance in northern Minnesota, USA. The color of each bar corresponds to the associated stability level in the legend and probability map. The percentages listed above each bar represent the percentage of total land area for each probability class in the study area.

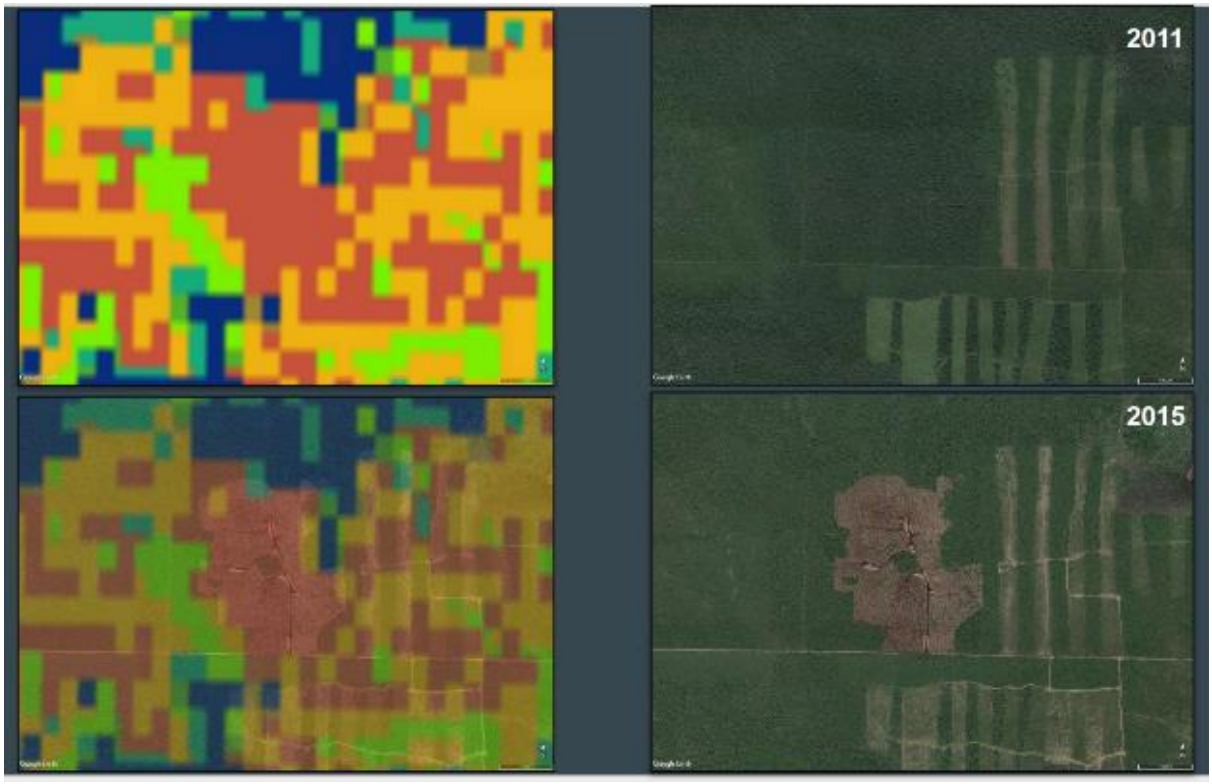

Figure 1.5. Detailed view of low level of classification stability in the class probability map. Forest disturbance in the form of harvest activity has occurred during the Forest Inventory and Analysis data collection cycle (2011 to 2015).

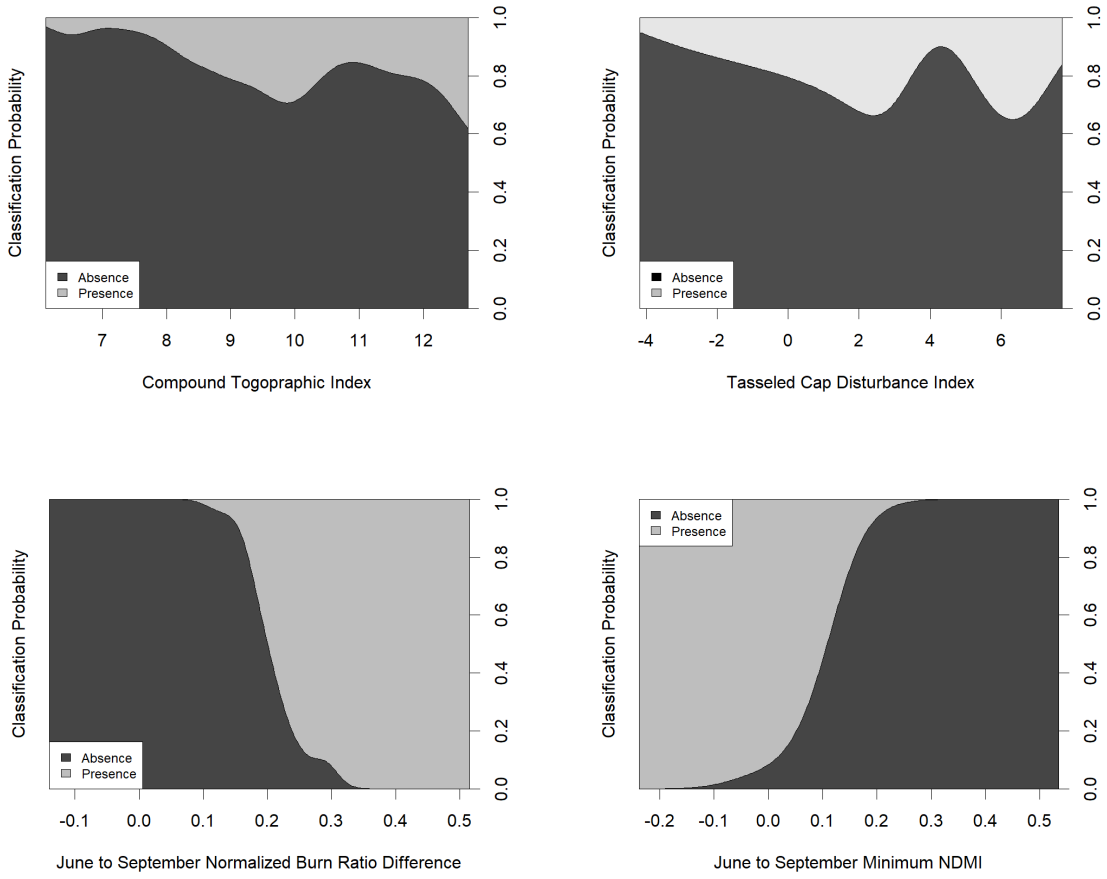

Figure 1.6. Conditional density plots for the top four predictors from the randomForest model. The light area represents the probability of presence and the shaded area represents the probability of absence across the range of values for each individual predictor.

Wolter et al (1995) used multi-date Landsat imagery in a partial least squares regression (PLS) to produce a mean class accuracy of 91% for black ash stands in northwestern Wisconsin after masking all non-hardwood and oak cover types. Wolter and White (2002) used the same methodology and data sources to map black ash cover in northeastern Minnesota with less success (overall accuracy = 83.5%). Again, with a PLS regression approach and multi-date Landsat, Wolter and Townsend (2011) estimated forest composition in northeastern Minnesota and produced a mean accuracy of 89.5% for black ash. Additional studies, focused more on black ash as a component of forest cover type, have generally shown lower classification accuracies. Reese et al (2002) achieved 81.8% accuracy when combining black ash and sugar maple in a "Broad leaf deciduous forest" class while mapping land cover in Wisconsin. Dillabaugh and King (2008) were unable to successfully classify any (0.0%) of a "Forest" type consisting of black ash and sugar maple in riparian system in Ontario, Canada but suffered due to a small sample size (n = 5). A study by Bergen et al (2007) in northern Michigan produced moderate success (accuracy = 75.8%) using a "Wet Deciduous" category that included aspen, red maple, black ash, and white birch.

Although direct comparisons cannot be made to the accuracies from models using regression instead of classification, previous studies on abundance have also included black ash at the species level. For example, Chambers et al (2013) reported an R^2 of 0.368 when estimating black ash basal area across eastern North America using forest inventory data combined with topographic, climate, and soil predictors in a multiple linear regression model. In contrast, Wilson et al (2013) found better success predicting black ash abundance (R^2 = 0.71) using data from MODIS with a nearest-neighbor imputation approach across the same study area. In methodologically related work, Dunckel et al (2015) reported an AUC = 0.91 when combining

relative basal area from FIA with climatic, soil, and Landsat data in a RF model to classify the presence and absence of a rare forest species (eastern hemlock) in Maine. Similarly, Evans and Cushman (2009) saw high model performance (≥ 0.98 AUC) for the classification of four conifer species in northern Idaho based on FIA data and using a downsampling technique in RF with predictors from topography, climate, and multispectral data.

Overall, the RF classification algorithm produced accurate classifications and generated an interpretable importance metric for each of the predictors used in the final model. Of the initial 44 predictors, only 12 remained after the model selection process. Of these 12 variables, CTI, TCAP DI, dNBR, and JSminNDMI were selected as the most important in the model as measured by mean decrease in accuracy (Figure 1.3). The conditional density plot for the most important predictor, CTI, indicated increasing values to be generally associated with an increasing likelihood of presence (Figure 1.6). As CTI values increase, drainage depressions tend to form on the landscape, giving the index strong correlations with soil moisture content and surface water pooling (Moore et al., 1991). The ability of CTI is discriminate these topographic features is important in defining the fundamental niche of black ash, characterized by saturated soils (i.e. bogs, streambanks) where few other tree species can establish or grow (Wright and Rauscher, 1990).

TCAP DI, a normalized, linear combination of the three standard tasseled cap indices (brightness, greenness, wetness), displayed a similar trend of values increasing in parallel with the likelihood of presence. Originally developed to highlight the spectral differences between vegetated and unvegetated pixels, TCAP DI scales with low values representing ‘mature’ forest to high values representing ‘bare soil’ (Healey et al., 2005). In its conditional density plot higher TCAP DI values are generally associated with a higher probability of presence (Figure 1.6). The

most likely explanation is the unique phenology of black ash relative to neighboring deciduous species. Black ash is often the last leaf-on and first leaf-off species (Wolter and Townsend, 2011), leading to less light being absorbed by its canopy. In their conditional density plots, distinct thresholds were evident for both dNBR and JSminNDMI (Figure 1.6). For dNBR, high values, representing more rapid senescence from April to October, were highly associated with black ash presence. For JSminNDMI, presence was associated with low values, which are often found in areas with sparser canopy closure, including forested wetland habitat. The base indices for these two metrics, NBR and NDMI, are both highly influenced by the inclusion of the mid-infrared (MIR) bands, which have been shown the ability to discriminate a gradient of foliar moisture content (Hunt et al., 1987).

Though model stability is high in much of the study area, the class probability map indicates low stability values occur over areas of disturbance, commonly from forest harvest (Figure 1.5). These areas likely account for the notable rate of false positives produced by the model. This may be due to unanticipated similarities in photosynthetic activity between areas of forest regrowth and black ash stands. Alternatively, classification confusion could be due to the temporal mismatch between the field data collection period (2011-2015) and the multispectral data (2015 only). To overcome these errors, the use of disturbance metrics from time-series data, such as those from Landtrendr (Kennedy et al., 2010), could be used to highlight changes in spectral trajectories indicative of significant vegetation change.

The classification produced in this study can be used to enhance forest management actions at local levels. Primarily, the map products are a complement to additional data sources used to assess the risks to black ash dominated ecosystems posed by EAB. Additionally, the map products may help identify locations for enhanced monitoring efforts investigating the possible

factors mitigating EAB impact, such as woodpecker habitat use (Flower et al., 2014, Lyons, 2015). The methods presented here could also be applied to models of presence and absence of other ash species across the anticipated invaded range of EAB. Dominant stands identified in this study may also be useful in establishing a baseline of black ash population health (Palik et al., 2011), helping to distinguish between periodic crown dieback and EAB infestation. Finally, these results could also complement the growing body of research assessing the early detection of EAB infestation through remote sensing. Previous work has investigated hyperspectral (Pontius et al., 2008; Zhang et al., 2014), LiDAR (Hu et al., 2014), and high-resolution data (Murfitt et al., 2016) but approaches utilizing time-series metrics and phenological signatures remain unexplored.

Conclusions

Known spatial limitations of systematically collected forest inventory data can be improved through the use of remotely sensed data in support of forest composition modelling and SAE. This study evaluated the efficacy of combining FIA survey data with spatial predictors from Landsat, LiDAR, and ancillary geospatial layers to classify black ash stand dominance in northern Minnesota, USA. The class-balanced RF modelling framework presented here achieved an overall accuracy of 85% and AUC of 0.92 (with class accuracies of 85.4% for absence and 85.7% for presence), indicating robust model performance. These results demonstrate the ability of remote sensing products to spatially extend forest survey data in support of land management at smaller management unit scales. The map outputs produced in this study can aid forest managers as they assess EAB risk and vulnerability in black ash dominated stands. Specifically,

these map outputs can be paired with hydrology, understory community, and wildlife data to anticipate local ecosystem impacts from the effects of rapid stand mortality due to EAB.

REFERENCES

Alonzo, M., Morton, D. C., Cook, B. D., Andersen, H. E., Babcock, C., & Pattison, R. (2017). patterns of canopy and surface layer consumption in a boreal forest fire from repeat airborne lidar. *Environmental Research Letters*, 12(6). http://doi.org/10.1088/1748-9326/aa6ade

Andersen, H. E., Barrett, T., Winterberger, K., Strunk, J., & Temesgen, H. (2009, May). Estimating forest biomass on the western lowlands of the Kenai Peninsula of Alaska using airborne lidar and field plot data in a model-assisted sampling design. In *Proceedings of the IUFRO Division 4 Conference: "Extending Forest Inventory and Monitoring over Space and Time* (pp. 19-22).

Bechtold, W. A., & Patterson, P. L. (2005). *The Enhanced Forest Inventory and Analysis Program — National Sampling Design and Estimation Procedures*. (W. A. Bechtold & P. L. Patterson, Eds.), *USDA General Technical Report* (Vol. SRS-80). http://doi.org/10.2737/SRS-GTR-80

BenDor, T. K., Metcalf, S. S., Fontenot, L. E., Sangunett, B., & Hannon, B. (2006). Modeling the spread of the Emerald Ash Borer. *Ecological Modelling*, *197*(1–2), 221–236. https://doi.org/10.1016/j.ecolmodel.2006.03.003

Bergen, K. M., & Dronova, I. (2007). Observing succession on aspen-dominated landscapes using a remote sensing-ecosystem approach. *Landscape Ecology*, 22(9), 1395–1410. http://doi.org/10.1007/s10980-007-9119-1

Blackard, J. A., Finco, M. V., Helmer, E. H., Holden, G. R., Hoppus, M. L., Jacobs, D. M., … Tymcio, R. P. (2008). Mapping U.S. forest biomass using nationwide forest inventory data and moderate resolution information. *Remote Sensing of Environment*, 112(4), 1658–1677. http://doi.org/10.1016/j.rse.2007.08.021

Breiman, L. (2001). Random forests. *Machine Learning*, *45*(1), 5–32. https://doi.org/10.1023/A:1010933404324

Chambers, D., Périé, C., Casajus, N., & de Blois, S. (2013). Challenges in modelling the abundance of 105 tree species in eastern North America using climate, edaphic, and topographic variables. *Forest Ecology and Management*, *291*, 20–29. https://doi.org/10.1016/j.foreco.2012.10.046

Chawla, N. V, Lazarevic, A., Hall, L. O., & Bowyer, K. (2003). SMOTEBoost: improving prediction of the minority class in boosting. In *Principles of Knowledge Discovery in Databases, PKDD-2003* (Vol. 2838, pp. 107–119). https://doi.org/10.1007/b13634

Chen, C., Liaw, A., & Breiman, L. (2004). *Using random forest to learn imbalanced data*. *University of California, Berkeley*. http://doi.org/ley.edu/sites/default/files/tech-reports/666.pdf

Clark, J. T., Fei, S., Liang, L., & Rieske, L. K. (2012). Mapping eastern hemlock: Comparing classification techniques to evaluate susceptibility of a fragmented and valued resource to an exotic invader, the hemlock woolly adelgid. *Forest Ecology and Management*, 266, 216–222. http://doi.org/10.1016/j.foreco.2011.11.030

Costanza, K. K. L., Livingston, W. H., Kashian, D. M., Slesak, R. A., Tardif, J. C., Dech, J. P., … Siegert, N. W. (2017). The Precarious State of a Cultural Keystone Species: Tribal and

Biological Assessments of the Role and Future of Black Ash. *Journal of Forestry*, (Lee 2004). https://doi.org/10.5849/jof.2016-034R1

Coulston, J. W., Moisen, G. G., Wilson, B. T., Finco, M. V, Cohen, W. B., & Brewer, C. K. (2012). Modeling Percent Tree Canopy Cover: A Pilot Study. *Photogrammetric Engineering & Remote Sensing*, 78(7), 715–727. http://doi.org/10.14358/PERS.78.7.715

Crook, D. J., Khrimian, A., Francese, J. A., Fraser, I., Poland, T. M., Sawyer, A. J., & Mastro, V. C. (2008). Development of a Host-Based Semiochemical Lure for Trapping Emerald Ash Borer Agrilus planipennis (Coleoptera: Buprestidae). *Environ. Entomol*, *37*(2), 356–365. https://doi.org/10.1603/0046-225x(2008)37[356:doahsl]2.0.co;2

Cutler, D. R., Edwards, T. C., Beard, K. H., Cutler, A., Hess, K. T., Gibson, J., & Lawler, J. J. (2007). Random forests for classification in ecology. *Ecology*, *88*(11), 2783–2792. http://doi.org/10.1890/07-0539.1

Dahl TE, Dick J, Swords J, Wilen BO (2009). Data collection requirements and procedures for mapping wetland, deepwater and related habitats of the United States. Division of habitat and resource conservation, national standards, and support team. U.S. Fish and Wildlife Service, Madison, p 85.

DeSantis, R. D., Moser, W. K., Gormanson, D. D., Bartlett, M. G., & Vermunt, B. (2013). Effects of climate on emerald ash borer mortality and the potential for ash survival in North America. *Agricultural and Forest Meteorology*, *178–179*, 120–128. https://doi.org/10.1016/j.agrformet.2013.04.015

Dillabaugh, K. A., & King, D. J. (2008). Riparian marshland composition and biomass mapping using lkonos imagery. *Canadian Journal of Remote Sensing*, 34(1–2), 143–158. http://doi.org/10.5589/m08-011

Drummond, C., & Holte, R. C. (2003). C4.5, class imbalance, and cost sensitivity: why under-sampling beats over-sampling. *Workshop on Learning from Imbalanced Datasets II*, 1–8. http://doi.org/10.1.1.68.6858

Duane, M. V., Cohen, W. B., Campbell, J. L., Hudiburg, T., Turner, D. P., & Weyermann, D. L. (2010). Implications of alternative field-sampling designs on landsat-based mapping of stand age and carbon stocks in Oregon forests. *Forest Science*, 56(4), 405–416. https://www.treesearch.fs.fed.us/pubs/37730

Dunckel, K., Weiskittel, A., Fiske, G., Sader, S. A., Latty, E., & Arnett, A. (2015). Linking remote sensing and various site factors for predicting the spatial distribution of eastern hemlock occurrence and relative basal area in Maine, USA. *Forest Ecology and Management*, *358*, 180–191. http://doi.org/10.1016/j.foreco.2015.09.012

Duveneck, M. J., Thompson, J. R., & Wilson, B. T. (2015). An imputed forest composition map for New England screened by species range boundaries. *Forest Ecology and Management*, *347*, 107–115. http://doi.org/10.1016/j.foreco.2015.03.016

Ellison, A. M., Bank, M. S., Clinton, B. D., Colburn, E. A., Elliott, K., Ford, C. R., … Webster, J. R. (2005). Loss of foundation species: consequences for the structure and dynamics of forested ecosystems. *Frontiers in Ecology and the Environment*, 3(9), 479–486. http://doi.org/10.1890/1540-9295(2005)003[0479:LOFSCF]2.0.CO;2

Evans, J. S., & Cushman, S. A. (2009). Gradient modeling of conifer species using random forests. *Landscape Ecology*, *24*(5), 673–683. http://doi.org/10.1007/s10980-009-9341-0

Evans, J. S., Murphy, M. A., Holden, Z. A., & Cushman, S. A. (2011). Modeling species distribution and change using random forest. In *Predictive Species and Habitat Modeling in Landscape Ecology: Concepts and Applications* (Vol. 86, pp. 139–159). New York, NY: Springer New York. http://doi.org/10.1007/978-1-4419-7390-0_8

Evans JS, Oakleaf J, Cushman SA, Theobald D (2014) An ArcGIS Toolbox for Surface Gradient and Geomorphometric Modeling, version 2.0-0. Accessed: April 5th, 2017. http://evansmurphy.wixsite.com/evansspatial/arcgis-gradient-metrics-toolbox

Falkowski, M. J., Evans, J. S., Martinuzzi, S., Gessler, P. E., & Hudak, A. T. (2009). Characterizing forest succession with lidar data: An evaluation for the Inland Northwest, USA. *Remote Sensing of Environment*, *113*(5), 946–956. http://doi.org/10.1016/j.rse.2009.01.003

Fassnacht, F. E., Latifi, H., Stereńczak, K., Modzelewska, A., Lefsky, M., Waser, L. T., … Ghosh, A. (2016). Review of studies on tree species classification from remotely sensed data. *Remote Sensing of Environment*, 186(8), 64–87. http://doi.org/10.1016/j.rse.2016.08.013

Flower, C. E., Knight, K. S., & Gonzalez-Meler, M. A. (2013). Impacts of the emerald ash borer (Agrilus planipennis Fairmaire) induced ash (Fraxinus spp.) mortality on forest carbon cycling and successional dynamics in the eastern United States. *Biological Invasions*, *15*(4), 931–944. https://doi.org/10.1007/s10530-012-0341-7

Flower, C. E., Long, L. C., Knight, K. S., Rebbeck, J., Brown, J. S., Gonzalez-Meler, M. A., & Whelan, C. J. (2014). Native bark-foraging birds preferentially forage in infected ash (Fraxinus

spp.) and prove effective predators of the invasive emerald ash borer (Agrilus planipennis Fairmaire). *Forest Ecology and Management*, 313, 300–306. http://doi.org/10.1016/j.foreco.2013.11.030

Gandhi, K. J. K., & Herms, D. A. (2010). Direct and indirect effects of alien insect herbivores on ecological processes and interactions in forests of eastern North America. *Biological Invasions*, *12*(2), 389–405. https://doi.org/10.1007/s10530-009-9627-9

Goerndt, M. E., Monleon, V. J., & Temesgen, H. (2013). Small-area estimation of county-level forest attributes using ground data and remote sensed auxiliary information. *Forest Science*, *59*(5), 536–548. https://doi.org/10.5849/forsci.12-073

He, H., & Garcia, E. A. (2009). Learning from imbalanced data. *IEEE Transactions on Knowledge and Data Engineering*, *21*(9), 1263–1284. https://doi.org/10.1109/TKDE.2008.239

Healey, S. P., Cohen, W. B., Zhiqiang, Y., & Krankina, O. N. (2005). Comparison of Tasseled Cap-based Landsat data structures for use in forest disturbance detection. *Remote Sensing of Environment*, *97*(3), 301–310. http://doi.org/10.1016/j.rse.2005.05.009

Herms, D. A., & McCullough, D. G. (2014). Emerald Ash Borer Invasion of North America: History, Biology, Ecology, Impacts, and Management. *Annual Review of Entomology*, *59*(1), 13–30. https://doi.org/10.1146/annurev-ento-011613-162051

Hu, B., Li, J., Wang, J., & Hall, B. (2014). The Early Detection of the Emerald Ash Borer (EAB) Using Advanced Geospacial Technologies. ISPRS - International Archives of the Photogrammetry, Remote Sensing, and Spatial Information Sciences, XL-2(October), 213–219. http://doi.org/10.5194/isprsarchives-XL-2-213-2014

Huang, C., Goward, S. N., Masek, J. G., Thomas, N., Zhu, Z., & Vogelmann, J. E. (2010). An automated approach for reconstructing recent forest disturbance history using dense Landsat time series stacks. *Remote Sensing of Environment*, 114(1), 183–198. http://doi.org/10.1016/j.rse.2009.08.017

Huete, A., Didan, K., Miura, T., Rodriguez, E. P., Gao, X., & Ferreira, L. G. (2002). Overview of the radiometric and biophysical performance of the MODIS vegetation indices. *Remote Sensing of Environment*, *83*(1–2), 195–213. http://doi.org/10.1016/S0034-4257(02)00096-2

Hunt, E. R., Rock, B. N., & Nobel, P. S. (1987). Measurement of leaf relative water content by infrared reflectance. *Remote Sensing of Environment*, 22(3), 429–435. http://doi.org/10.1016/0034-4257(87)90094-0

Japkowicz, N., & Stephen, S. (2002). The class imbalance problem: A systematic study. *Intelligent Data Analysis*, *6*(5), 429–449. Retrieved from http://iospress.metapress.com/content/MXUG8CJKJYLNK3N0

Justice, C. O., Vermote, E., Townshend, J. R., Defries, R., Roy, D. P., Hall, D. K., ... & Lucht, W. (1998). The Moderate Resolution Imaging Spectroradiometer (MODIS): Land remote sensing for global change research. *IEEE Transactions on Geoscience and Remote Sensing*, *36*(4), 1228-1249.https://doi.org/10.1109/36.701075

Kenis, M., Auger-Rozenberg, M. A., Roques, A., Timms, L., Péré, C., Cock, M. J. W., … Lopez-Vaamonde, C. (2009). Ecological effects of invasive alien insects. In *Ecological Impacts of Non-Native Invertebrates and Fungi on Terrestrial Ecosystems* (Vol. 11, pp. 21–45). Dordrecht: Springer Netherlands. https://doi.org/10.1007/978-1-4020-9680-8_3

Kennedy, R. E., Yang, Z., & Cohen, W. B. (2010). Detecting trends in forest disturbance and recovery using yearly Landsat time series: 1. LandTrendr - Temporal segmentation algorithms. Remote Sensing of Environment, 114(12), 2897–2910. http://doi.org/10.1016/j.rse.2010.07.008

Klooster, W. S., Herms, D. A., Knight, K. S., Herms, C. P., McCullough, D. G., Smith, A., … Cardina, J. (2014). Ash (Fraxinus spp.) mortality, regeneration, and seed bank dynamics in mixed hardwood forests following invasion by emerald ash borer (Agrilus planipennis). *Biological Invasions*, *16*(4), 859–873. https://doi.org/10.1007/s10530-013-0543-7

Knight, K. S., Brown, J. P., & Long, R. P. (2013). Factors affecting the survival of ash (Fraxinus spp.) trees infested by emerald ash borer (Agrilus planipennis). *Biological Invasions*, *15*(2), 371–383. https://doi.org/10.1007/s10530-012-0292-z

Kolka, R., D'Amato, A., Wagenbrenner, J., Slesak, R., Pypker, T., Youngquist, M., … Palik, B. (2018). Review of Ecosystem Level Impacts of Emerald Ash Borer on Black Ash Wetlands: What Does the Future Hold? *Forests*, *9*(4), 179. https://doi.org/10.3390/f9040179

Kovacs, K. F., Mercader, R. J., Haight, R. G., Siegert, N. W., McCullough, D. G., & Liebhold, A. M. (2011). The influence of satellite populations of emerald ash borer on projected economic costs in U.S. communities, 2010-2020. *Journal of Environmental Management*, *92*(9), 2170–2181. https://doi.org/10.1016/j.jenvman.2011.03.043

Liang, L., & Fei, S. (2014). Divergence of the potential invasion range of emerald ash borer and its host distribution in North America under climate change. *Climatic Change*, *122*(4), 735–746. https://doi.org/10.1007/s10584-013-1024-9

Liaw, A., & Wiener, M. (2002). Classification and Regression by randomForest. *R News*, *2*(December), 18–22.

Liu, C., Zhang, L., Davis, C. J., Solomon, D. S., Brann, T. B., & Caldwell, L. E. (2003). Comparison of neural networks and statistical methods in classification of ecological habitats using FIA data. *Forest Science*, *49*(4), 619–631. https://academic.oup.com/forestscience/article/49/4/619/4617526

Liu, W., Song, C., Schroeder, T. A., & Cohen, W. B. (2008). Predicting forest successional stages using multitemporal Landsat imagery with forest inventory and analysis data. *International Journal of Remote Sensing*, 29(13), 3855–3872. http://doi.org/10.1080/01431160701840166

Lovett, G. M., Weiss, M., Liebhold, A. M., Holmes, T. P., Leung, B., Lambert, K. F., … Weldy, T. (2016). Nonnative forest insects and pathogens in the United States: Impacts and policy options. *Ecological Applications*, *26*(5), 1437–1455. https://doi.org/10.1890/15-1176

Lyons, D. B. (2015). What's killing the green menace: mortality factors affecting the emerald ash borer (Coleoptera: Buprestidae) in North America? The Canadian Entomologist, 147(3), 263–276. http://doi.org/10.4039/tce.2014.62

Martin, M. E., Newman, S. D., Aber, J. D., & Congalton, R. G. (1998). Determining Forest Species Composition Using High Spectral Resolution Remote Sensing Data. *Remote Sensing of Environment*, 65(3), 249–254. http://doi.org/10.1016/S0034-4257(98)00035-2

McRoberts, R. E. (2009). A two-step nearest neighbors algorithm using satellite imagery for predicting forest structure within species composition classes. *Remote Sensing of Environment*, 113(3), 532–545. http://doi.org/10.1016/j.rse.2008.10.001

McRoberts, R. E., & Tomppo, E. O. (2007). Remote sensing support for national forest inventories. Remote Sensing of Environment, 110(4), 412–419. https://doi.org/10.1016/j.rse.2006.09.034

MN DNR. 2017. *ECS: Laurentian Mixed Forest Province: Minnesota DNR.* Minnesota Department of Natural Resources, accessed April 25th, 2017. http://www.dnr.state.mn.us/ecs/212/index.html

MNGeo. 2017. *Metadata: LiDAR Elevation, Arrowhead Region, NE Minnesota, 2011*. Minnesota Department of Natural Resources, accessed April 25th, 2017. http://www.mngeo.state.mn.us/chouse/metadata/lidar_arrowhead2011.html

Moisen, G. G., Freeman, E. A., Blackard, J. A., Frescino, T. S., Zimmermann, N. E., & Edwards, T. C. (2006). Predicting tree species presence and basal area in Utah: A comparison of stochastic gradient boosting, generalized additive models, and tree-based methods. *Ecological Modelling*, *199*(2), 176–187. https://doi.org/10.1016/j.ecolmodel.2006.05.021

Moore, I. D., Grayson, R. B., & Ladson, A. R. (1991). Digital terrain modelling: A review of hydrological, geomorphological, and biological applications. *Hydrological Processes*, *5*(1), 3–30. https://doi.org/10.1002/hyp.3360050103

Murfitt, J., He, Y., Yang, J., Mui, A., & De Mille, K. (2016). Ash decline assessment in emerald ash borer infested natural forests using high spatial resolution images. *Remote Sensing*, 8(3), 256. http://doi.org/10.3390/rs8030256

Murphy, M. A., Evans, J. S., & Storfer, A. (2010). Quantifying Bufo boreas connectivity in Yellowstone National Park with landscape genetics. *Ecology*, *91*(1), 252–261. http://doi.org/10.1890/08-0879.1

Nelson, M. D., Healey, S. P., Moser, W. K., & Hansen, M. H. (2009). Combining satellite imagery with forest inventory data to assess damage severity following a major blowdown event in northern Minnesota, USA. *International Journal of Remote Sensing*, 30(19), 5089–5108. http://doi.org/10.1080/01431160903022951

Ohmann, J. L., & Gregory, M. J. (2002). Predictive mapping of forest composition and structure with direct gradient analysis and nearest- neighbor imputation in coastal Oregon, U.S.A. *Canadian Journal of Forest Research*, *32*(4), 725–741. http://doi.org/10.1139/x02-011

Palik, B. J., Ostry, M. E., Venette, R. C., & Abdela, E. (2012). Tree regeneration in black ash (Fraxinus nigra) stands exhibiting crown dieback in Minnesota. *Forest Ecology and Management*, *269*, 26–30. https://doi.org/10.1016/j.foreco.2011.12.020

Poland, T. M., & McCullough, D. G. (2006). Emerald ash borer: Invasion of the urban forest and the threat to North America's ash resource. *Journal of Forestry*, *104*(3), 118–124.

Pontius, J., Martin, M., Plourde, L., & Hallett, R. (2008). Ash decline assessment in emerald ash borer-infested regions: A test of tree-level, hyperspectral technologies. *Remote Sensing of Environment*, 112(5), 2665–2676. http://doi.org/10.1016/j.rse.2007.12.011

Powell, S. L., Cohen, W. B., Healey, S. P., Kennedy, R. E., Moisen, G. G., Pierce, K. B., & Ohmann, J. L. (2010). Quantification of live aboveground forest biomass dynamics with Landsat time-series and field inventory data: A comparison of empirical modeling approaches. *Remote Sensing of Environment*, 114(5), 1053–1068. http://doi.org/10.1016/j.rse.2009.12.018

Qi, J., Chehbouni, A., Huete, A. R., Kerr, Y. H., & Sorooshian, S. (1994). A modified soil adjusted vegetation index. *Remote Sensing of Environment*, *48*(2), 119–126. http://doi.org/10.1016/0034-4257(94)90134-1

R Development Core Team, 2017. R: A Language and Environment for Statistical Computing.

Reese, H. M., Lillesand, T. M., Nagel, D. E., Stewart, J. S., Goldmann, R. A., Simmons, T. E., … Tessar, P. A. (2002). Statewide land cover derived from multiseasonal Landsat TM data. *Remote Sensing of Environment*, 82(2–3), 224–237. http://doi.org/10.1016/S0034-4257(02)00039-1

Schroeder, T. A., Healey, S. P., Moisen, G. G., Frescino, T. S., Cohen, W. B., Huang, C., … Yang, Z. (2014). Improving estimates of forest disturbance by combining observations from landsat time series with U.S. Forest Service Forest Inventory and Analysis data. *Remote Sensing of Environment*, 154(1), 61–73. http://doi.org/10.1016/j.rse.2014.08.005

Sheridan, R., Popescu, S., Gatziolis, D., Morgan, C., & Ku, N.-W. (2014). Modeling Forest Aboveground Biomass and Volume Using Airborne LiDAR Metrics and Forest Inventory and Analysis Data in the Pacific Northwest. *Remote Sensing*, 7(1), 229–255. http://doi.org/10.3390/rs70100229

Slesak, R. A., Lenhart, C. F., Brooks, K. N., D'Amato, A. W., & Palik, B. J. (2014). Water table response to harvesting and simulated emerald ash borer mortality in black ash wetlands in Minnesota, USA. *Canadian Journal of Forest Research*, *44*(8), 961–968. https://doi.org/10.1139/cjfr-2014-0111

Soil Survey Staff. Gridded Soil Survey Geographic (gSSURGO) Database for Minnesota. United States Department of Agriculture, Natural Resources Conservation Service. Available online at https://gdg.sc.egov.usda.gov/. *April 12, 2017* (FY2015 official release).

Telander, A. C., Slesak, R. A., D'Amato, A. W., Palik, B. J., Brooks, K. N., & Lenhart, C. F. (2015). Sap flow of black ash in wetland forests of northern Minnesota, USA: Hydrologic implications of tree mortality due to emerald ash borer. *Agricultural and Forest Meteorology*, *206*, 4–11. https://doi.org/10.1016/j.agrformet.2015.02.019

Thompson, S. D., Nelson, T. A., White, J. C., & Wulder, M. A. (2015). Mapping Dominant Tree Species Over Large Forested Areas Using Landsat Best-Available-Pixel Image Composites. *Canadian Journal of Remote Sensing*, *41*(3), 203–218. https://doi.org/10.1080/07038992.2015.1065708

USGS. 2017. "Earth resources observation and science (EROS) center science processing architecture (ESPA) on demand interface." *Department of Interior, U.S. Geological Survey. Product Guide Version 4.0,* accessed April 5, 2017 from https://landsat.usgs.gov/sites/default/files/documents/espa_odi_userguide.pdf

Vogeler, J. C., Braaten, J. D., Slesak, R. A., & Falkowski, M. J. (2018). Extracting the full value of the Landsat archive: Inter-sensor harmonization for the mapping of Minnesota forest canopy

cover (1973–2015). *Remote Sensing of Environment*, 209(January), 363–374. http://doi.org/10.1016/j.rse.2018.02.046

Willow, A. J. (2011). Indigenizing Invasive Species Management: Native North Americans and the Emerald Ash Borer (EAB) Beetle. *Culture, Agriculture, Food, and Environment*, *33*(2), 70–82. http://doi.org/10.1111/j.2153-9561.2011.01051.x

Wilson, B. T.; Lister, A. J.; Riemann, R. I.; Griffith, D. M. (2013). Live tree species basal area of the contiguous United States (2000-2009). Newtown Square, PA: USDA Forest Service, Rocky Mountain Research Station. https://doi.org/10.2737/RDS-2013-0013

Wolter, P. T., Mladenoff, D. J., Host, G. E., & Crow, T. R. (1995). Improved forest classification in the northern Lake States using multi-temporal landsat imagery. *Photogrammetric Engineering and Remote Sensing*, 61(9), 1129–1143.

Wolter, P. T., & White, M. A. (2002). Recent forest cover type transitions and landscape structural changes in northeast Minnesota, USA. *Landscape Ecology*, 17(2), 133–155. http://doi.org/10.1023/A:1016522509857

Wolter, P. T., & Townsend, P. A. (2011). Multi-sensor data fusion for estimating forest species composition and abundance in northern Minnesota. *Remote Sensing of Environment*, *115*(2), 671–691. http://doi.org/10.1016/j.rse.2010.10.010

Wright, J. W., & Rauscher, H. M. (1990). Fraxinus nigra Marsh. black ash. In *Silvics of North America volume 2: Hardwoods* (Vol. 2, pp. 344–347). USDA Forest Service. Retrieved from https://www.na.fs.fed.us/spfo/pubs/silvics_manual/volume_2/fraxinus/nigra.htm

Youngquist, M. B., Eggert, S. L., D'Amato, A. W., Palik, B. J., & Slesak, R. A. (2017). Potential Effects of Foundation Species Loss on Wetland Communities: A Case Study of Black Ash Wetlands Threatened by Emerald Ash Borer. *Wetlands*, *37*(4), 787–799. https://doi.org/10.1007/s13157-017-0908-2

Zhang, K., Hu, B., & Robinson, J. (2014). Early detection of emerald ash borer infestation using multisourced data: a case study in the town of Oakville, Ontario, Canada. *Journal of Applied Remote Sensing*, 8(1), 83602. http://doi.org/10.1117/1.JRS.8.083602

Zimmermann, N. E., Edwards, T. C., Moisen, G. G., Frescino, T. S., & Blackard, J. A. (2007). Remote sensing-based predictors improve distribution models of rare, early successional, and broadleaf tree species in Utah. *Journal of Applied Ecology*, 44(5), 1057–1067. http://doi.org/10.1111/j.1365-2664.2007.01348.x

CHAPTER 2: ESTIMATING CANOPY FUEL ATTRIBUTES FROM LOW-DENSITY LIDAR

Introduction

Simulations of wildland fire risk and fire behavior are important components of forest management. Confidence in these simulations is dependent on the accuracy and operational relevance of spatial data inputs describing major drivers of wildland fire, including canopy fuels. The spatial data currently available, through programs such as LANDFIRE, are useful at national and regional levels; However, the spatial resolution and accuracy of these products often are insufficient to support fire modeling and planning needs at local levels. Fortunately, active remote sensing techniques, such as LiDAR, can produce accurate, high-resolution estimates of forest structure that often partially govern fire activity. In this study, the efficacy of low-density LiDAR data, together with a canopy cover estimate from Landsat time-series data, were combined in randomForest *k*-nearest neighbor imputation approach to estimate canopy bulk density, two measures of canopy base height, and stand age across the Boundary Waters Canoe Area in northern Minnesota, USA. This method produced strong relationships between the estimates of canopy fuel attributes and field-based data for stand age (R^2 = 0.82, RMSE = 10.12 years), crown fuel base height (R^2 = 0.79, RMSE = 1.10 m), live crown base height (R^2 = 0.71, RMSE =1.60 m), and canopy bulk density (R^2 = 0.58, RMSE = 0.09kg/m^3). In contrast, a standard randomForest model was less successful in generating estimates of canopy height (R^2 = 0.33, RMSE = 2.08 m). These results suggest that low-density LiDAR can be used to estimate several canopy fuel attributes in a mixed forest ecosystem, with accuracies much improved over existing data products from sources such as LANDIFRE. The map products generated from this

research will provide local forest managers with cost-efficient and operationally ready data required to simulate fire behavior and support management efforts.

Background

Wildland fire is an important natural feature of forested ecosystems. Recently, the frequency and extent of severe fires have increased in many areas of the United States, influenced in part by historically large fuel loads and increased stand densities generated through fire suppression activities (Agee and Skinner, 2005; Keane et al., 2002). Compounding this problem, projected climate scenarios indicate further increases in fire frequency and severity likely due to warming temperatures (van Mantgem, et al., 2013), changes in fire season length (Westerling et al., 2006; 2016), and increasing drought stress (Littel et al., 2016).

To protect people and property at high risk from wildland fire (those at or near the wildland-urban interface), federal agencies spent $2.9 billion on fire suppression in 2017 (NIFC, 2018). The ability of land managers to mitigate the cost and scale of this threat depends the understanding of fire behavior as predicted by mathematical models of fire spread such as FARSITE (Finney, 2004) and FlamMap (Finney, 2006). Simulating fire growth and spread with these models requires detailed, accurate knowledge of the spatial patterns and extent of surface and canopy vegetation structures relating to fuel availability (Keane et al., 2001).

Common canopy fuel attributes include: canopy bulk density (CBD), canopy base height (CBH), and canopy height. These metrics contribute to the understanding of the initiation and spread of crown fires, which are often more severe and difficult to control as compared to surface fires (Scott and Reinhardt, 2001). CBD is a metric that does not have a universally

accepted calculation but generally attempts to quantify per unit volume of combustible live and dead canopy fuel available (Scott and Reinhardt, 2001). Similarly, measures of CBH are not universally defined but generally refer to the height at which a tree canopy exceeds a minimum fuel load threshold. Fire behavior models use CBD and CBH to determine the threshold for active crown fire initiation (Finney, 2004) as well as an indication of potential fire spread between stands (Riaño et al., 2004b). Canopy height influences wind direction and speed through stands, influencing spotting through the movement of embers (Finney, 2004).

As a complement to CBH and CBD, knowledge of stand age class and distribution offers additional insight into crown fire dynamics in forested landscapes. In pre-fire contexts, stand age can help to describe flammability relationships (Tiribelli, et al., 2018) and ignition potential (Erni et al., 2018). In post-fire contexts, stand age can inform the understanding of wildlife habitat selection (Wood, et al., 2018), species recruitment (Kalamees et al., 2005), and burn severity in forest regeneration planning (Taylor et al., 2014).

Field-based measurement of forest fuels for operational use is costly and often logistically impractical across large spatial extents. Fortunately, remotely sensed data can be used in support of forest fuel quantification and fire risk management. To achieve this, forest managers often rely on fuels layers available from the LANDFIRE program, a nation-wide mapping project utilizing Landsat imagery and field data to generate spatial estimates of forest fuels in the United States at a 30 m spatial resolution using a Classification and Regression Tree modelling approach (Rollins, 2009). However, these products are designed to provide regional and national baselines and are not recommended to replace locally available products with higher spatial resolutions (Reeves et al., 2006). Previous studies comparing the efficacy of local data to LANDFIRE products have indicated that the latter tend to under-predict fire initiation in behavioral models

(Krasnow et al., 2009) and are poorly correlated with field measurements relative to estimates produced with local data or with more advanced machine learning algorithms (Pierce et al., 2012). These shortcomings are also caused in part by inadequate sampling densities at local extents and the inability of moderate-resolution remotely sensed data (Landsat) to capture the complex, three-dimensional structural heterogeneity of canopy fuels (Reeves et al., 2009).

To overcome these limitations, high-resolution data from remote sensing-based systems can be used in tandem with locally available field-based measurements to generate accurate, spatially-explicit, and cost-effective products that quantify and map fire fuels, ultimately supporting fire management decision making. Data from LiDAR (light detection and ranging) offers a detailed descriptions of three-dimensional forest structure and improves upon the limitations of passive sensors, which are not overly sensitive to forest structure (Lefsky et al., 2001; Wagner et al., 2008). It has been well established in the literature that LiDAR can assist in modeling a variety of forest attributes including basal area (Lefsky et al., 1999; Falkowski et al., 2010; Fekety et al., 2015; Hudak et al., 2006, 2008), biomass (Boudreau et al., 2008; Lefsky et al., 1999; Zhao et al., 2009), leaf area index (Morsdorf et al., 2006; Riaño et al., 2004a; Tang et al., 2014), and successional stage (Falkowski et al., 2009), among others. LiDAR has also been successful used to generate estimates of canopy fuel attributes including overall canopy height (Erdody and Moskal, 2010; Hermosilla et al., 2014; Skowronski et al., 2007), canopy base height (Popescu and Zhao, 2008; Zhao et al., 2011), canopy bulk density (González-Ferreiro et al., 2014; Riaño et al., 2004b), canopy cover (Hall et al., 2005; Riaño, 2003), and stand age (Racine et al., 2014).

Many of the previously mentioned studies make use of medium to high density LiDAR (2 to 16 points/m^2) and are limited in their spatial extent due to logistical and/or financial constraints

associated with LiDAR data collection across large areas. Collecting LiDAR data across entire states or regions often results in lower point densities and are often intended to support surface elevation characterization rather than vegetation mapping. As a result, acquisition parameters of LiDAR with densities less than 2 pts/m^2 have been described as sub-optimal for the characterization of forest structure. However, a handful of studies have demonstrated the efficacy of low-density LiDAR in forestry applications. For example, Montagnoli et al (2015) used a point density of less than 2 pts/m^2 to model biomass in a mixed broad leaf forest in northern Italy, achieving accuracies of $R^2 = 0.76$. Shendryk et al (2014) combined low density LiDAR (average 0.8 pts/m^2) with optical imagery to model biomass in a mixed forest in southern Sweden, and demonstrated model performance of $R^2 = 0.80$. A study by Treitz et al 2012 compared low (0.5 pts/m^2) to high density (3.6 pts/ m^2) LiDAR data and found little difference in predictive accuracy for eight different forest attributes. Even with extremely low densities (0.035 pts/m^2), Thomas et al (2006) accurately estimated mean height, biomass, and basal area in a forest area in southwestern Ontario, Canada.

Even with these encouraging examples, the application of low-density LiDAR (< 1 point/m^2) to estimate canopy fuels is not well represented in the literature, especially in mixed forest systems. And despite low-density collections accounting for 43% of publicly available LiDAR in the United States (Department of Commerce, 2018), these datasets often are produced without specific vegetation mapping and modeling goals. To expand the scope of research and make use of readily available data, more research is needed to evaluate if low-density LiDAR can support vegetation mapping efforts. To meet this need, this study evaluated the efficacy of low-density LiDAR data to estimate canopy fuels in structurally complex mixed forests in northern Minnesota, USA. Specifically, this study used a randomForest imputation modeling framework

to predict canopy fuel attributes of interest to forest managers, including canopy base height, canopy bulk density, canopy height, and stand age. To generate a parsimonious model, a model selection procedure was performed, maximizing ecological interpretability as measured by variable importance. Because the end products are direct inputs to models of fire behavior and fire risk, imputation accuracy was compared against traditionally utilized data resources, such as LANDFIRE.

Methods

Study Area

The study area covers 14,000 km^2 in northern Minnesota, USA (Figure 2.1) and encompasses the Boundary Waters Canoe Area (BWCA). Elevation ranges from 337 to 701 m above mean sea-level. Pleistocene glacial till formed much of the soil structure in the BWCA with mineral soil conditions ranging from granitic deposits to sandy loams (Heinselman, 1996). Located in a transition zone between deciduous hardwoods and true northern boreal forests, the vegetation and biophysical characteristics of the BWCA are diverse. Conifers and deciduous tree species exist along a spectrum between pure and mixed stands of pine, fir, aspen, and maple trees. Charcoal in lake sediments has indicated that these stands were historically subject to frequent fire events (Swain, 1973) but after the implementation of 20^{th} century forest management practices this frequency declined dramatically (Heinselman, 1996).

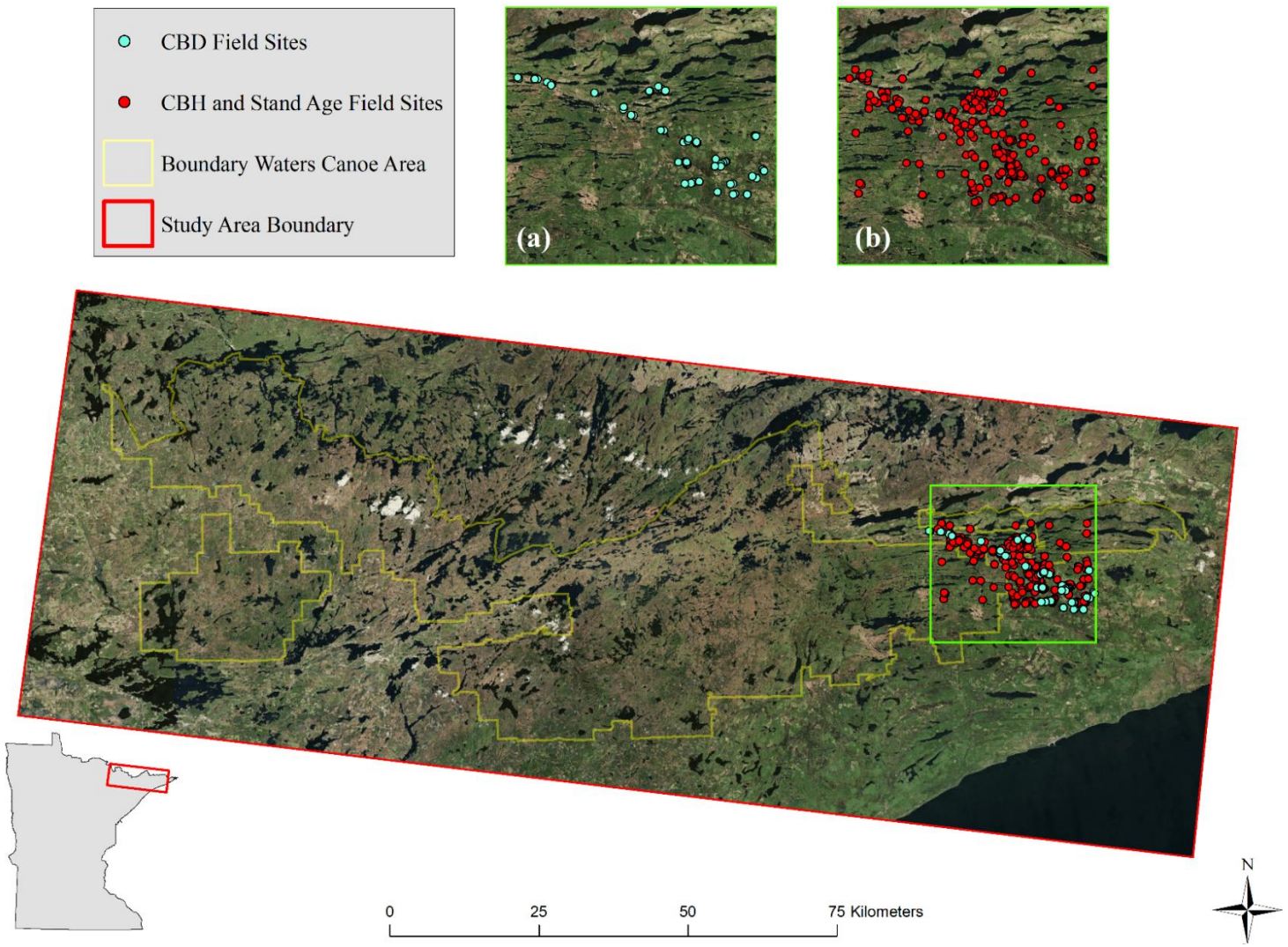

Figure 2.1. Location map displaying the study area in northern Minnesota, USA. Also shown is the extent of the Boundary Waters Canoe Area and the location of the field data used in the study.

Sampling design and data collection

Fuels data for canopy height, CBH and age were collected at 263 inventory plots within the study area during the summers of 2014 and 2015. Plot locations were located using a stratified random sampling design, where strata were defined by forest type and stand age classes. Plot locations were randomized within the study area in known forest stands > 30 years old and > 4.05 ha (10 acres). No plots were allowed within 24 m (80 ft.) of a stand boundary or 80 feet (~24 m) from another plot. Forest inventory crews installed 0.04 ha ($1/10^{th}$ acre) fixed-radius forest inventory plots and recorded standard forest inventory data (i.e., individual tree measurements of species, height, and DBH) and additional plot-level measurements of stand age and canopy base height. Plots were located on the ground using handheld Trimble Juno GPS devices and differentially corrected to enhance the accuracy of final plot locations. For this study, stand age was determined by selecting and coring the oldest tree from the dominant species present on each plot. CBH was assessed by two separate metrics: crown fuel base height (CFBH) and live crown base height (LCBH). CFBH is defined as a measure of height above the ground of the lowest live and/or dead fuels that can move fire higher in the tree. LCBH is defined as height above ground to the base of the live crown.

For CBD, a separate sample of 60 inventory plots were surveyed in 2015 and 2016. These plots were randomly located within the study area but within 2 km of a paved road and within a forested area. Plots were located on the ground using handheld Trimble GeoXT GPS devices and differentially corrected. At each plot, field crews recorded average canopy gap fraction (CGF), average and total species basal area, and average canopy height. A LAI-2000 instrument was used to record CGF in a square 3 x 3 grid of nine points arranged around the plot center, each separated by five meters, following Keane et al (2005). With the LAI-2000, a 38° angle was used

Table 2.1. Names and descriptions of the five calculation methods evaluated in the development of the canopy bulk density (CBD) mode. Units for all CBD measurements are in kg/m^3.

CBD Method	Description
TREEWISE	Based on total needle and large branch biomass sum of all conical tree volumes on a plot.
PLOTWISE	Based on total needle and large branch biomass and the 23-degree LAI2000 view angle and estimated forest height for the plot (kg/m^3)"
KEANE	Calculated using Keane et al. (2005) formula for use with weighted LAI2000 GAP measurements (CBD_E = 0.0402 + 7.6293 * LAI2000)
CONE	Total plot CBD based on cone shape of trees
CYL	Plotwise total CBD based on cylinder shapes of trees

with average canopy height to determine the respective CGF plot radius. Within this CGF-defined circular plot area, all conifers species > 15 cm DBH were measured for height, height to first live branch, and canopy diameter. These data were used with published allometry (Perala and Alban, 1993) to calculate component biomass estimates for each field plot (i.e., needles, branch, and bole). The variety and detail of these measurements (i.e. biomass, CGF) allowed for the use of five CBD estimation methods (Table 2.1). These methods provide only indirect estimates and none are universally applicable to every forest type. Therefore, to determine the most appropriate CBD estimation method, only the most accurate of the five different methods tested was retained for continued evaluation.

Remote sensing data

LiDAR data used in the study was collected May 14th to June 1, 2011 by Woolpert, Inc. under contract from the State of Minnesota as a part of the Minnesota Elevation Mapping Project (MEMP). The expected outcome of the MEMP was the development of a state-wide, high-accuracy surface elevation dataset with possible vegetation mapping applications left unexplored. Horizontal positional accuracy of the dataset is +/-1.6 m ($\alpha = 0.05$) and vertical positional accuracy is 3.6 cm ($\alpha = 0.05$) with a minimum side-lap of 25% and a scan angle of ± 20° off nadir (MNGEO, 2017). The average density of the LiDAR point cloud is 0.44 pts/m^2.

To characterize the horizontal and vertical distribution of vegetation a suite of raster grid metrics were created from the LiDAR point cloud data (Table 2.3) using the FUSION software package (McGaughey, 2012) at a 10 m spatial resolution. Due to the narrow side lap in the flight path and large scan angle, these metrics were visually screened for data quality issues before inclusion in the final predictor list. LiDAR canopy cover layers were replaced by a Landsat time-series derived canopy cover product generated from the work of Vogeler et al (2018) due to striping between flight lines. For this substitute data, spectral indices were harmonized across all Landsat sensors along with photo-interpreted samples of canopy cover to produce annual maps of predicted canopy cover across the state from 1973-2015 (Vogeler et al., 2018). The map of canopy cover for 2011 was chosen for use in all models to best match the year of LiDAR data collection.

Model development

A randomForest (RF; Breiman, 2001) *k*-nearest neighbor imputation approach (RF-kNN), available in the "yaImpute" R package (Crookston et al., 2007), was used to develop models of

four canopy fuel attributes: stand age, CFBH, LCBH, and CBD. RF-kNN is different from other imputation methods because it identifies nearest neighbor distances based on proximity values generated from an initial RF model (Hudak et al., 2008). Furthermore, comparative studies of nearest neighbor methods have shown RF-kNN to be a preferable modeling approach when predicting forest attributes (Eskelson et al., 2009; Hudak et al., 2008, 2014; Latifi and Koch, 2012; Latifi et al., 2010; Packalén et al., 2010; Powell et al., 2010).

Following Falkowski et al. (2009), model parsimony was optimized during the implementation of the RF-kNN approach to maximize the ecological interpretability of the model results. First, using the 'rfUtilities' package in R (Evans and Murphy, 2017; Evans et al., 2011), a Gram-Schmidt QR decomposition was performed to identify and remove multicollinear variables. Next, to generate parsimonious RF models an iterative selection function was performed using the 'modelSel' function in the 'rfUtilities' package (Murphy et al., 2010). This function generates a Model Improvement Ratio (MIR) statistic that describes how well predictor variables minimize the mean squared error and maximize the variation explained in the response. The RF model generating the highest MIR values is then identified as the most parsimonious model.

Using parsimony optimized predictor sets and associated RF proximity values, kNN imputations were run to generate predicted values to compare against the training data for LCBH, CFBH, CBD, and stand age. For the imputations, the number of neighbors was set to k = 1, a value understood to preserve the distribution and covariance structure of the reference dataset (Franco-Lopez, et al., 2001). Canopy fuel attributes were then imputed across the study area at a 10 m resolution. In a separate analysis, canopy height was evaluated only after the

Table 2.2. The 55 predictors evaluated in the model development of the five canopy fuel attributes. Selected predictors in the final models for crown fuel base height (CFBH), live crown base height (LCBH), canopy bulk density (CBD), stand age, and canopy height (CH) are indicated with 'X'.

Predictor Name	Description	CFBH	LCBH	CBD	Age	CH
FRET	Percentage of first returns above mean height	X				
HCV	Coefficient of variation of heights				X	
LMOM1	First L-moment (Hosking, 1990)	X	X	X		
LMOM2	Second L-moment (Hosking, 1990)					
LMOM3	Third L-moment (Hosking, 1990)			X	X	X
LMOM4	Fourth L-moment (Hosking, 1990)					
LCV	L-moment coefficient of variation		X			
LSKEW	L-moment skewness					
MEDMAD	Median absolute deviation from median height	X	X			
MEDMODE	Median absolute deviations from mode height	X				
H5PCT	Average height 5th percentile					
H10PCT	Average height 10th percentile	X				
H20PCT	Average height 20th percentile	X				
H25PCT	Average height 25th percentile					
H30PCT	Average height 30th percentile					
H40PCT	Average height 40th percentile			X		X
H50PCT	Average height 50th percentile			X		X
H60PCT	Average height 60th percentile			X		X
H70PCT*	Average height 70th percentile					
H75PCT*	Average height 75th percentile					
H80PCT*	Average height 80th percentile					
H90PCT*	Average height 90th percentile					
H95PCT*	Average height 95th percentile					
H99PCT	Average height 99th percentile				X	X
HMEAN*	Average height of returns					
CRR	Canopy relief ratio (mean-min)/(max-min)		X			
HCUBE*	Cubic mean of all return heights					
HSKEW	Kurtosis of heights					
HMAX*	Maximum height					
HQUAD*	Quadratic mean height					
HSTD*	Standard deviation of all return heights					
HVAR	Variance of heights			X		
STRATUM1	Percentage of vegetation returns > 0.15 m and ≤ 1 m					X
STRATUM2	Percentage of vegetation returns > 1 m and ≤ 2 m					
STRATUM3	Percentage of vegetation returns > 2 m and ≤ 3 m	X			X	
STRATUM4_MEAN	Mean height of vegetation returns >3 m and ≤ 5 m	X				
STRATUM4	Percentage of vegetation returns >3 m and ≤ 5 m	X	X		X	X
STRATUM4_SD	Standard deviation of vegetation returns >3 m and ≤ 5 m	X		X		
STRATUM5_MEAN	Mean height of vegetation returns > 5 m and ≤ 10 m	X	X			
STRATUM5	Percentage of vegetation returns > 5 m and ≤ 10 m	X	X	X	X	X
STRATUM5_SD	Standard deviation of vegetation returns > 5 m and ≤ 10 m	X				X
STRATUM6	Percentage of vegetation returns >10 m and ≤ 20 m		X			X
STRATUM6_SD	Standard deviation of vegetation returns 10 m and ≤ 20 m		X			X
STRATUM7_MEAN	Mean height of vegetation returns >20 m and ≤ 30 m					
STRATUM7	Percentage of vegetation returns > 20 m and ≤ 30 m					
STRATUM7_SD	Standard deviation of vegetation returns > 20 m and ≤ 30 m					
STRATUM8_MEAN*	Mean height of vegetation returns >30 m and ≤ 45 m					
STRATUM8*	Percentage of vegetation returns > 30 m and ≤ 45 m					
STRATUM8_SD*	Standard deviation of vegetation returns > 30 m and ≤ 45 m					
ASPECT	Aspect					
PLANCURV	Surface planar curvature					
PROFCURV	Surface profile curvature				X	
SLOPE	Slope	X	X	X		
SRI	Solar radiation index			X		
CCLST	Canopy cover derived from Landsat time-series		X		X	

* indicates identified as multicollinear

initial RF model selection process. To examine the potential for bias due to scan angle, residuals from the canopy height model were explored as a function of average scan angle and height variability.

Model performance and evaluation

The performance of each model was assessed by comparing imputed predictions to observed values in the training dataset and evaluating accuracy using the coefficient of determination (R^2) and root mean square error (RMSE). Performance for the canopy height model was assessed directly from the R^2 and RMSE values produced by the RF model summary. The five methods of estimating CBD were analyzed and the method that produced the highest R^2 was retained as the final CBD model.

The influence of individual predictors in each model was analyzed in two ways. First, internal RF variable importance was generated to measure the mean decrease in accuracy if a predictor was removed from the model. Second, partial dependence plots were generated for the most important predictors in each model. In the context of RF modeling, partial dependence plots represent an attempt to visualize the relationship between the response variable and the marginal effect of a single predictor while accounting for the average effect of all other predictors used to grow the forest of regression trees (Cafri and Bailey, 2016; Cutler et al., 2007).

Results

Model selection and variable importance

The QR-Decomposition procedure identified and removed 13 multicollinear predictors (Table 2.3), leaving 42 potential model metrics to use in model selection. The canopy height model retained 11 total predictors including: return heights (H40PCT, H50PCT, H60PCT, H99PCT), pulse densities (STRATUM1, STRATUM4, STRATUM5, STRATUM6), and the third *L*-moment (Table 2.3). The stand age model retained 11 predictors (Figure 2.2): mid-canopy pulse densities (STRATUM3, STRATUM4, STRATUM5), return heights (H99PCT), surface texture (SRI, PROFCURV), as well as the Landsat time-series derived canopy cover layer (CCLST; Table 2.3). The CFBH model retained 16 predictors (Figure 2.3): the first *L*-moment, mid-canopy pulse densities (STRATUM3, STRATUM4, STRATUM5, STRATUM6), return heights (H10PCT, H20PCT), among others (Table 2.3). The LCBH model retained 11 predictors (Figure 2.3): *L*-moments (LMOM1, LMOM3), mid-canopy pulse densities (STRATUM4, STRATUM5, STRATUM6), height distribution characteristics (MEDMAD, CRR), slope, and canopy cover (CCLST; Table 2.3). Plot-wise cylinder volume (CYL; Table 2.1) was identified as the best of the five CBD estimation methods (Figure 2.4) and the final CBD model retained 11 total predictors (Figure 2.3) including: mid-canopy pulse densities (STRATUM4, STRATUM5, STRATUM6), return heights (H40PCT, H50PCT, H60PCT, HVAR), surface texture (SRI), slope, and *L*-moments (LMOM1, LMOM3; Table 2.3).

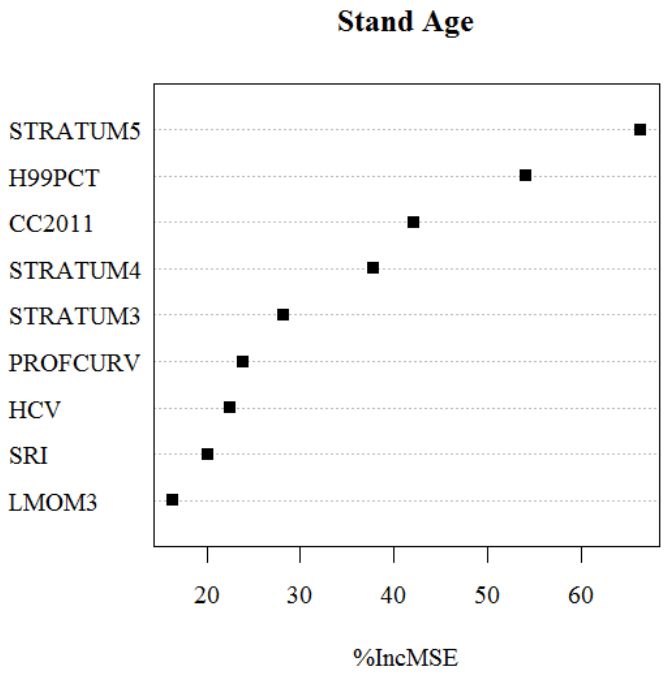

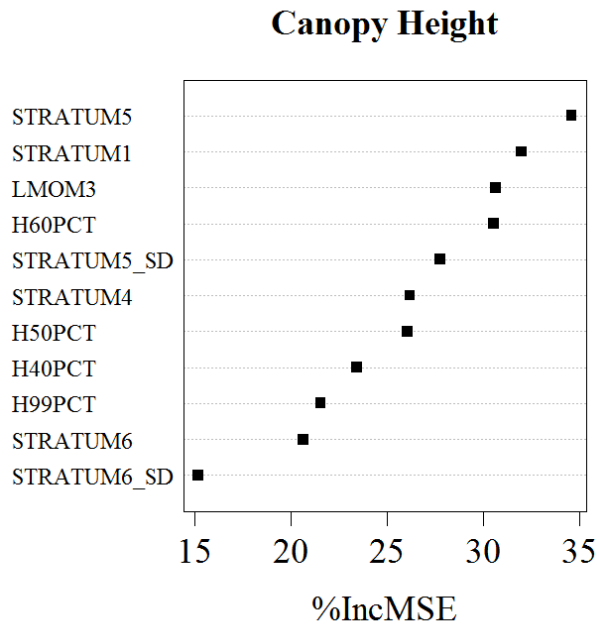

Figure 2.2. Variable importance plots from the randomForest models of stand age and canopy height. '%IncMSE' indicates the percent increase in mean squared error if the predictor was removed from the model.

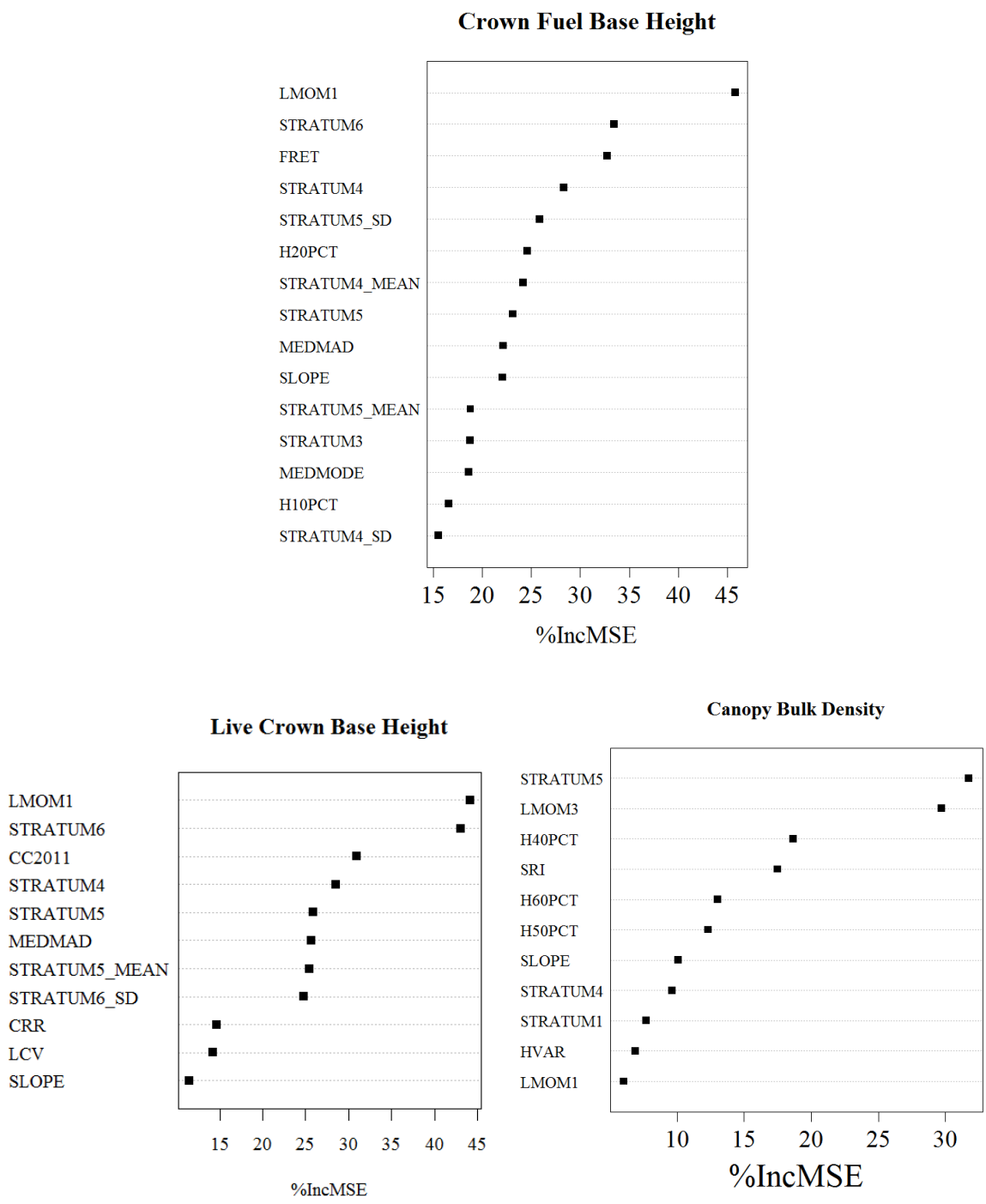

Figure 2.3. Variable importance plots from the randomForest models of crown fuel base height, live crown base height, and canopy bulk density. '%IncMSE' indicates the percent increase in mean squared error if the predictor was removed from the model.

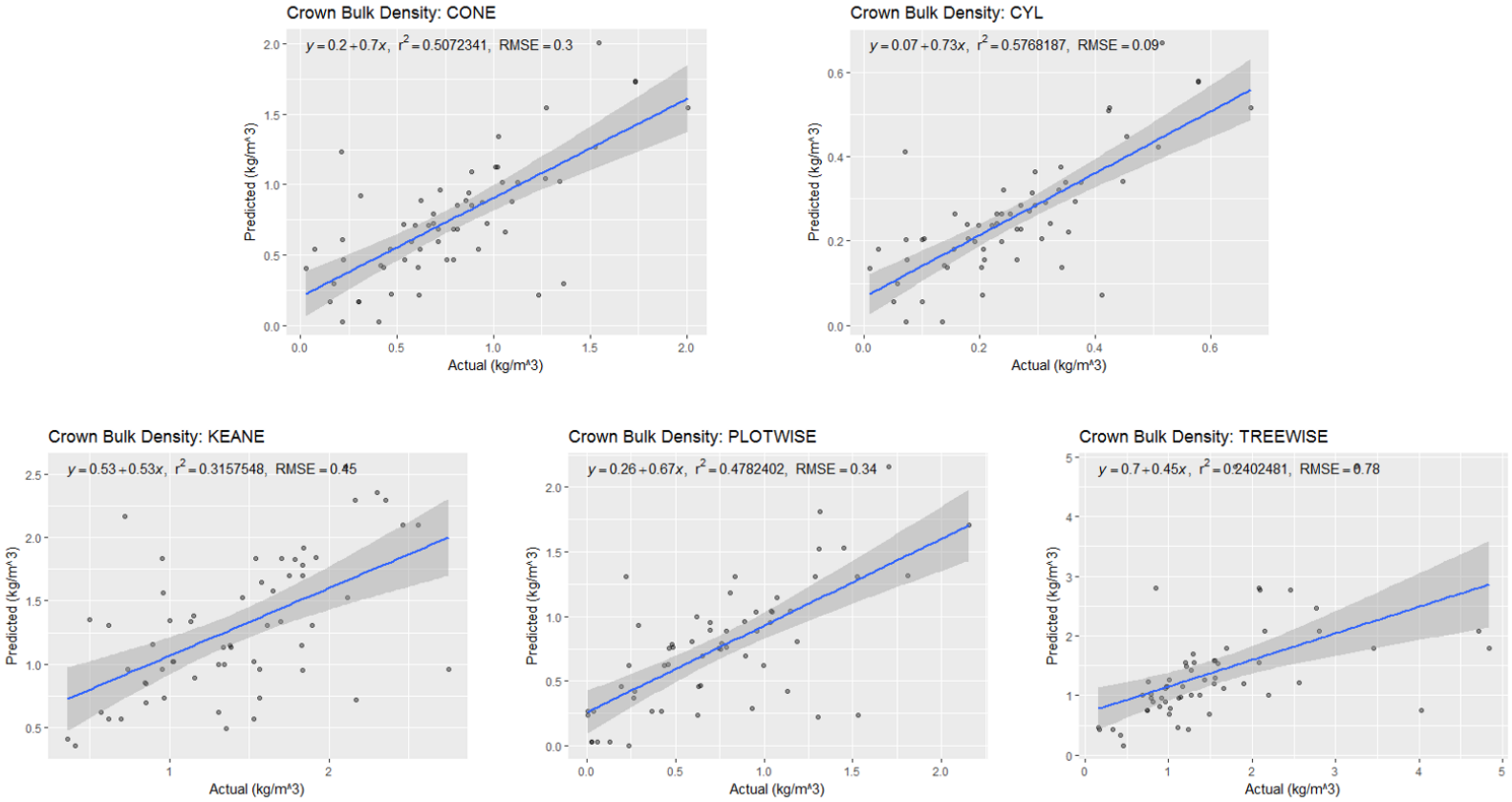

Figure 2.4. Comparisons of randomForest k-nearest neighbor imputation model performance for the five candidate canopy bulk density measurement methods. The least squares fit trend line is shown in blue and the trend line standard error is shown as a transparent gray polygon.

Model performance and evaluation

Overall, the imputation models of canopy fuels showed strong relationships (Figure 2.4) between predicted and field plot data for stand age (R^2 = 0.82, RMSE = 10.12 years), CFBH (R^2= 0.79, RMSE = 1.10 m), LCBH (R^2= 0.71, RMSE = 1.60 m), and CBD (R^2= 0.58, RMSE = 0.09 kg/m^3). Canopy height showed the weakest modeled relationship between predicted and actual values (R^2= 0.33, RMSE = 2.08 m).

Additional analysis showed no relationship between the canopy height model residuals, average scan angle, and canopy height variability.

In terms of variable importance, the proportion of fifth strata returns (STRATUM5) and average return heights in the 99th percentile (H99PCT) were the most important for the stand age model (Figure 2.2). In the canopy height model, the most important predictors (Figure 2.2) were the proportion of returns from the fifth and first strata (STRATUM5, STRATUM1). For the CFBH and LCBH models, the most important predictors (Figure 2.3) were identical: the proportion of returns from the sixth strata (STRATUM6) and the first *L*-moment (LMOM1). In the CBD model, the most important predictors (Figure 2.3) were the percentage of returns in the fifth strata (between 5 - 10 m) and the third *L*-moment (LMOM3).

To determine the marginal effect of important variables (as determined by RF), partial dependence plots were examined for each canopy fuel attribute model. For the CFBH and LCBH models, the first *L*-moment (LMOM1) values and the proportion of sixth strata returns (STRATUM6) are both associated with increasing heights (Figure 2.6). For the CBD model, STRATUM5 values are associated with increasing biomass volumes while the third L-moment is associated with higher biomass volumes for values from ~ -0.5 to 0.5 (Figure 2.7). For the stand age model, the proportion of fifth strata returns (STRATUM5) are associated with variations in

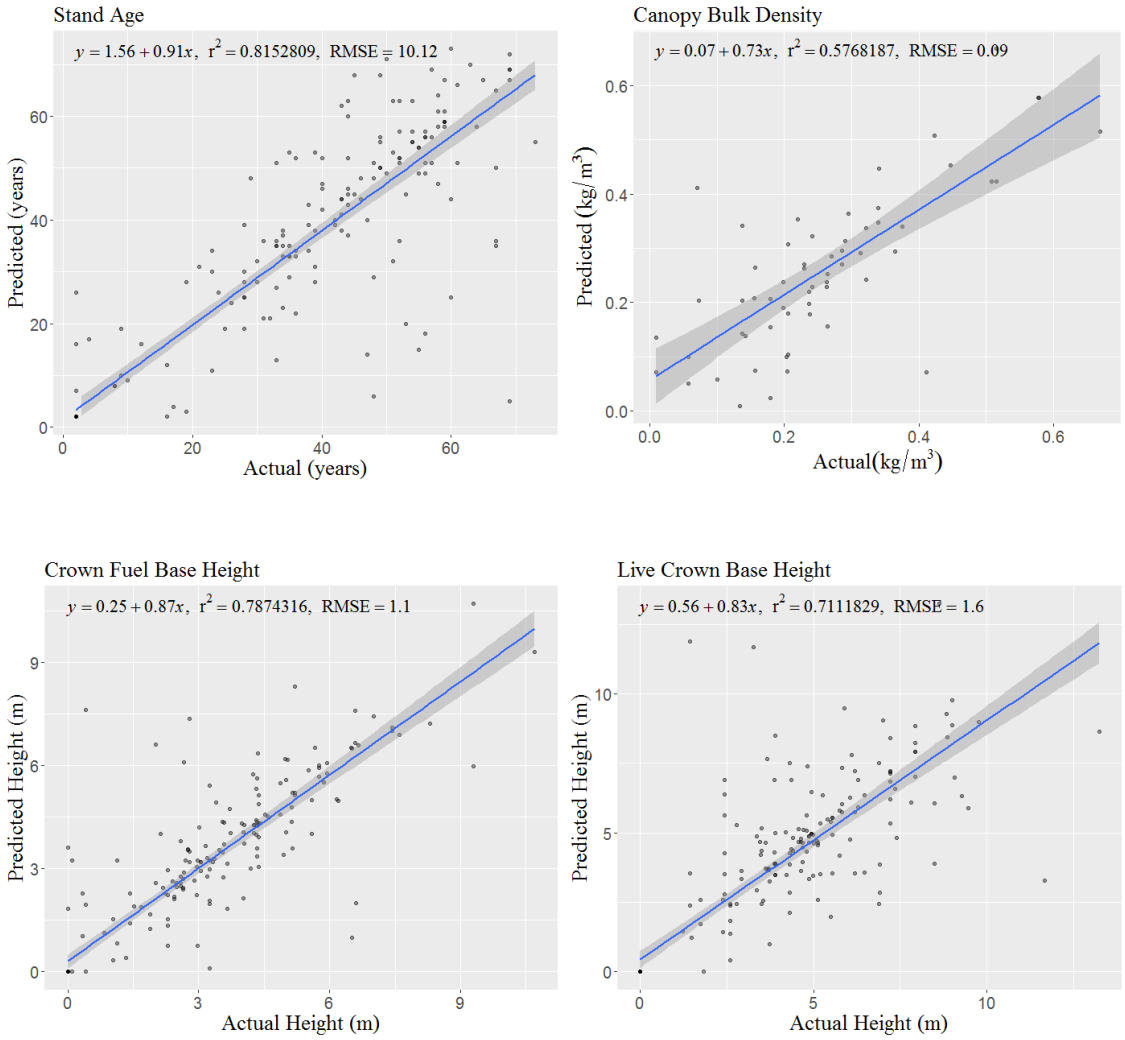

Figure 2.5. Plots comparing predicted versus observed values for each of the four imputed canopy fuel attributes. Accuracy metrics are displayed in the form of the coefficient of determination (R^2) and the root mean squared error (RMSE). The lease squares fit trend line is shown in blue and the trend line standard error is shown as a transparent gray polygon.

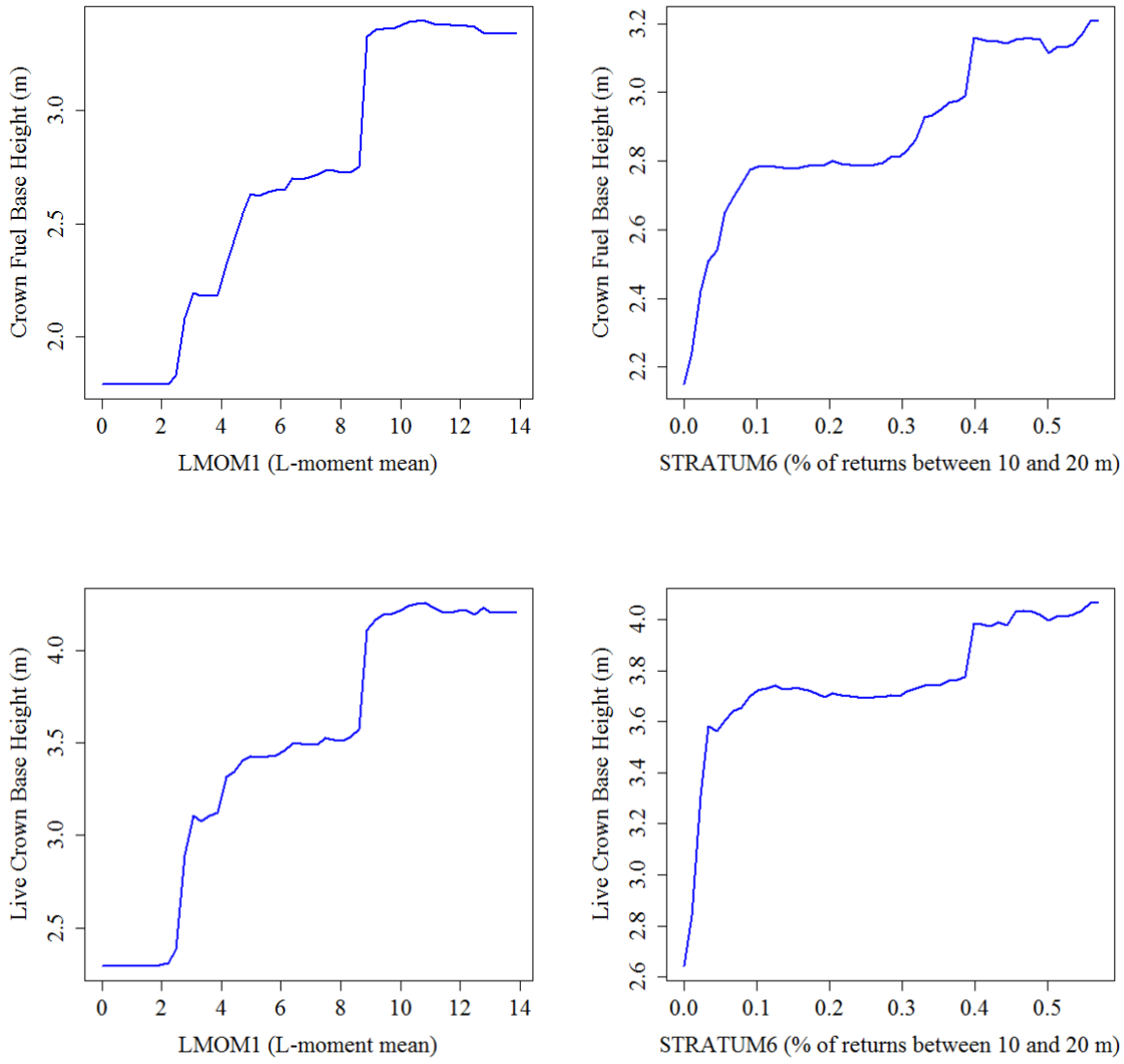

Figure 2.6. Partial dependence plots describing the marginal effects of the top two predictors from randomForest models of crown fuel base height and live crown base height.

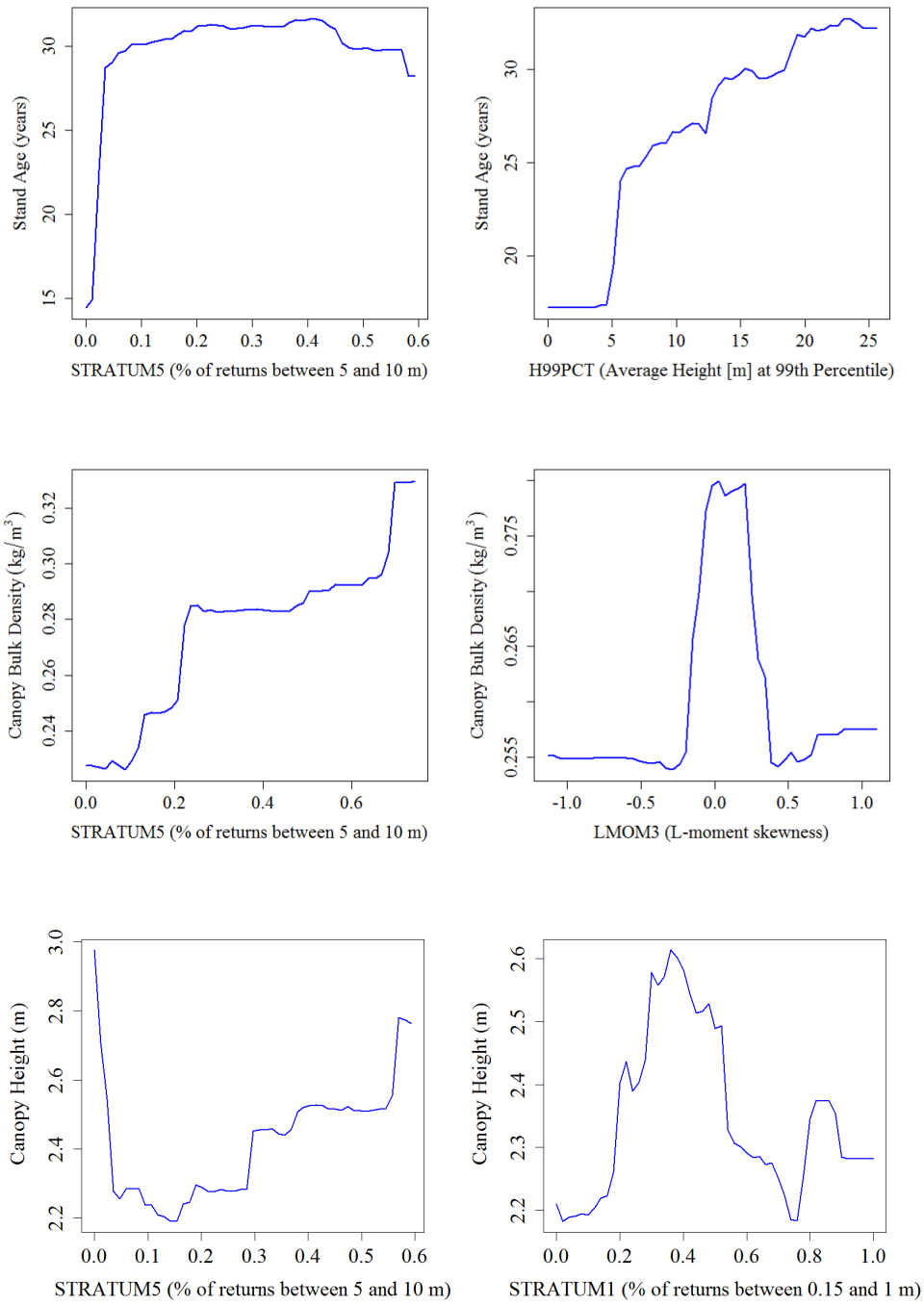

Figure 2.7. Partial dependence plots describing the marginal effects of the top two predictors from randomForest models of stand age, canopy bulk density, and canopy height.

older stand ages while 99th percentile return heights (H99PCT) are associated with increasing stand ages (Figure 2.7). For the canopy height model, increasing STRATUM5 and STRATUM1 values between ~ 0.2 and 0.6 are both associated with increasing heights (Figure 2.7).

Discussion

The RF-kNN models developed in this study demonstrate the ability of low-density LiDAR to effectively describe several canopy fuels attributes in a mixed forest setting. Imputed estimates of CFBH, LCBH, CBD, and stand age facilitated the production of detailed, high-resolution maps (Figure 2.8) ready for use as fire behavior model inputs while the RF model of canopy height underperformed. The imputed products improve upon the accuracies and spatial limitations found in commonly utilized canopy fuels data sources, such as LANDFIRE.

The accuracies presented in this study offer similar results compared to the few previous studies estimating CBH and CBD using low-density LiDAR (< 1 pts/m^2). Maguya et al. (2014) presented R^2 ranging from 0.46 to 0.75 for CBH at a density of 0.5 pts/m^2 in conifer-dominated forests of eastern Finland. González-Ferreiro et al. (2014) generated estimates for CBD (R^2 = 0.44) in *Pinus radiata* stands in northwest Spain also at 0.5 pts/m^2. However, González-Ferreiro et al. (2014) also reported CBH accuracy in upwards of R^2 = 0.96.

Accuracies also met or exceed results from studies using LiDAR pulse densities much higher than those presented here. For example, Andersen et al (2005) attained an R^2 of 0.77 when estimating CBH from LiDAR data with a point density of 3.5 pts/m^2 for in a small forest in southwestern Washington dominated by Douglas fir. Hermosilla et al. (2014) achieved similar CBH results in another Douglas fir forest in northwestern Oregon (R^2: 0.78) from LiDAR with a

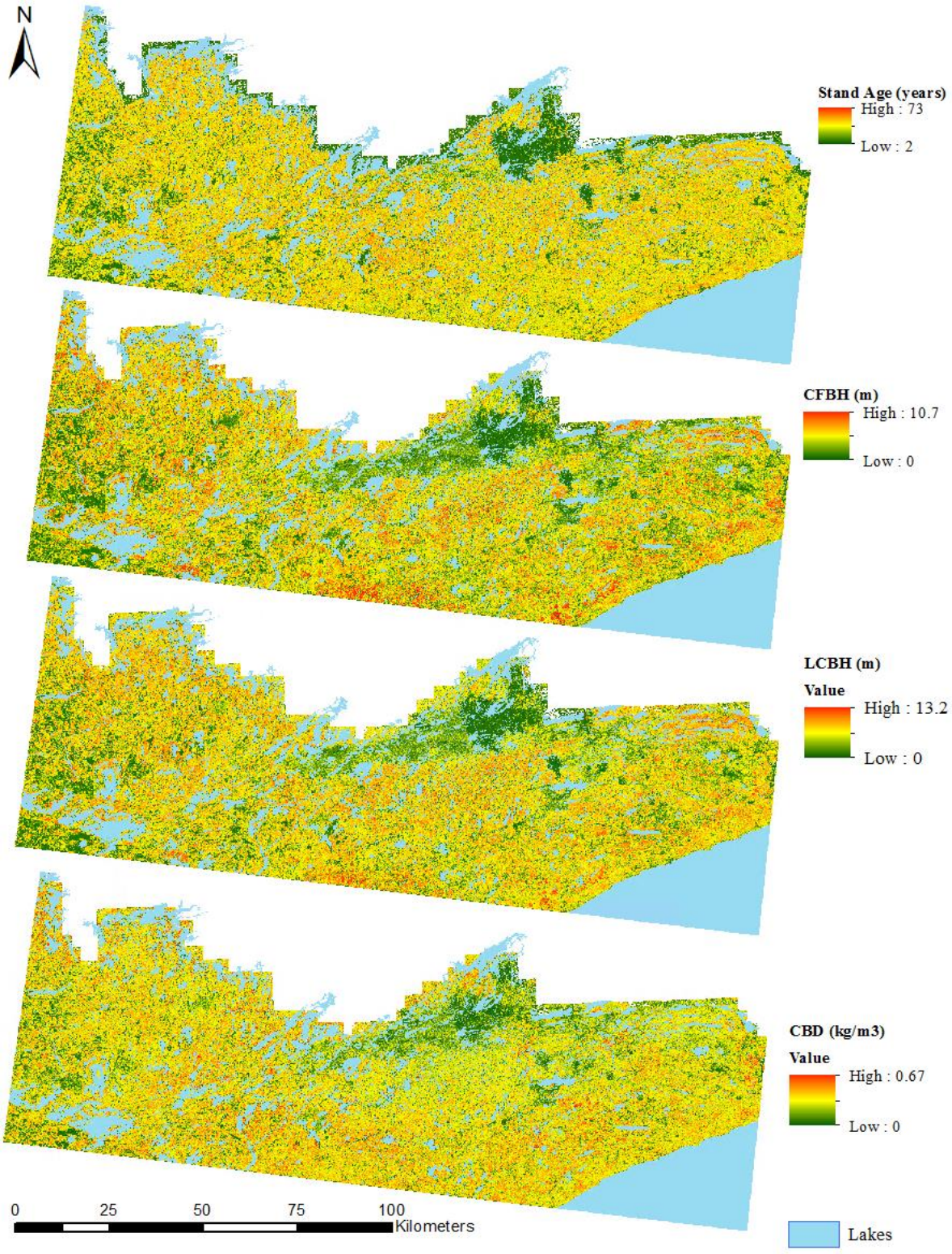

Figure 2.8. Imputation predictions across the study area for stand age, crown fuel base height (CFBH), live crown base height (LCBH), and canopy bulk density (CBD).

density of 8 pts/m^2. Ermody and Moskal (2010) reported accuracies ranging from R^2 = 0.77 to 0.84 for CBH in the eastern Cascade mountains of Washington using a LiDAR dataset with a density of 4 pts/m^2. These high-density LiDAR studies all achieved higher R^2 values for CBD (0.67 to 0.88) and canopy height (0.79 to 0.98). However, it should be noted that direct comparisons to these particular studies warrant caution due to their use of square root and log transformations of dependent variables.

This study's accuracy is also comparable or outperforms previous studies using metrics derived from LiDAR to estimate stand age. Work by Racine et al. (2014) is very similar in accuracy (R^2: 0.83), model methodology (RF-kNN imputation), and study system (northern boreal transition forest in Quebec, Canada). Additional work by Straub and Koch (2011) combined LiDAR with multispectral data but had less success (R^2 = 0.63) in a mixed forest site in southern Germany. Unfortunately, direct comparisons to other studies are limited because stand age is more often segmented into discrete classes of successional stage (i.e. Falkowski et al., 2009; Kane et al., 2010) as opposed to a continuous response variable.

Using an RF-kNN imputation approach provides for the assessment of predictor importance as measured by mean decrease in accuracy (Figures 2.2, 2.3). Of the original 55 predictor variables, only one, describing the proportion of returns between 5 and 10 m (STRATUM5), was retained across all models. This finding is consistent with previous studies that have previously identified canopy strata intensities as important across multiple models of forest attributes (Bright et al., 2017, González-Olabarria et al., 2012). For the models of CFBH and LCBH, the most important variables are identical (LMOM1, STRATUM6). Similar marginal effects of each predictor are found in the partial dependence plots for the CFBH and LCBH models (Figure 2.6), where the importance of STRATUM6 (pulse density proportion between 10

and 20 m) can be explained by many CFBH and LCBH values falling within the height range of this strata.

The fact that LMOM1 was also shared by the CFBH and LCBH models is perhaps more intriguing due to recent research regarding the improved understanding of forest structure through the use of *L*-moments (Valbuena et al., 2017). LMOM1 is functionally analogous to mean canopy height, a metric identified as an important component of other crown fuel models (Ermody and Moskal, 2010; Hermosilla et al., 2014; Riaño et al., 2004b). The efficacy of *L*-moments over conventional moments may be explained by the former's robustness to the smaller sample sizes and outliers (Hosking, 1990) such as those found in low-density LiDAR point cloud data.

For CBD, the top predictors were STRATUM5 and LMOM3 (an L-moment analogous to skewness). The partial dependence plot of CBD and STRATUM5 (Figure 2.7) indicates that the number of mid-canopy returns generally increases as the amount of tree biomass becomes denser between 5 and 10 meters. The plot of LMOM3 to CBD (Figure 2.7) indicates increasing biomass volumes are associated with returns distributed mostly through the mid-crown heights. As the number of returns concentrate at higher or lower heights, biomass values decrease. However, it should be noted that the variation of the marginal effect on CBD occurs over a narrow range (0.255 to 0.280 kg/m^3). For the stand age model, the most important predictors were STRATUM5 and H99PCT (the average height of the 99^{th} percentile of returns). The known relationship between age and tree height (King, 1990) is supported by the importance of H99PCT in the stand age model and the association of H99PCT with increasing stand ages in the partial dependence plot (Figure 2.7). The partial dependence plot for STRATUM5 and stand age (Figure 2.7) appears to indicate the power of this predictor lies mainly in its ability to distinguish

between zero and non-zero values of stand age (i.e. forested vs. non-forested conditions). Finally, for canopy height and STRATUM5, increasing heights track with increasing pulse densities at higher heights similar to LCBH and CFBH (Figure 2.7). The narrow range of STRATUM1 (the proportion of returns between 0.15 and 1 m) values associated with increasing canopy heights (Figure 2.7) may reflect differences in forest vegetation types. The deliverables for this project did not originally include canopy height models and it remains unclear if the model results reflect differences in precision between canopy height and canopy base height field measurements.

Despite numerous studies of forest attributes using LiDAR, previous research has focused heavily on conifer-dominated systems (Lim et al., 2003). This may be partially driven by concerns over the variability of leaf-off, leaf-on conditions in forests with deciduous components or a concentration of research in locations with available funding for LiDAR data collection efforts. However, previous research has shown little difference in model accuracy due to the timing of LiDAR acquisition (Anderson and Bolstad, 2013; Wasser et al., 2013; White et al., 2015) and LiDAR collections occur across a wide variety of forest conditions in the United States. Indeed, data covering mixed forest systems have been used estimate biomass (Hoover, et al., 2018; Li et al., 2014 Lim et al., 2003; Zheng et al., 2008), stem density (Hawbaker et al., 2010) and basal area (Hayashi et al., 2014; Woods et al., 2008). Results from this study contribute to this body of work while addressing a lack of research into LiDAR-based canopy fuel estimates in mixed forest systems.

Studies characterizing canopy structure have shown only small differences in accuracy and precision between high and low-density LiDAR collections (Jakubowski et al., 2013, Lim et al., 2008; Treitz et al., 2012). This bodes well for areas where statewide, low-density LiDAR

data is already available, offering a cost-effective complement to expensive, time-consuming, and logistically complex field-based sampling. These results highlight the valuable ecological knowledge that can be generated even when LiDAR collection efforts are not specifically intended for vegetation mapping, as was the case with the Minnesota Elevation Mapping Project. The canopy fuels estimates produced in this study improve upon the accuracy and resolution found in nationwide spatial data resources of canopy fuels, such as LANDFIRE. Indeed, the accuracies presented here show a marked improvement over LANDFIRE for CBH ($R^2 = 0.45$) and are comparable to CBD ($R^2 = 0.58$) for the Lake States region. Additionally, field data used in this study was poorly correlated with LANDFIRE data for CBH and CBD (R^2 range: 0.01 - 0.30). The improvement in accuracy is likely influenced by LiDAR's ability to describe the three-dimensional structure of forest canopies whereas LANDFIRE is reliant on imagery from two-dimensional optical sensors. High-resolution data from LiDAR also leads to more detailed spatial inputs for fire modeling and more relevant information for local, operational forest management.

Although the results of this study demonstrate the utility of low-density LiDAR, it is worth pointing out that two aspects of the initial data collection effort may have hindered model performance. The LiDAR data was collected with a minimum side-lap of 25%, which less than the 50% often seen in other collection efforts. Low or inconsistent side-lap can influence overall point densities. The wide scan angle of the LiDAR collection (20 degrees) may have also led to the striping seen during the initial visual assessment of the potential predictors because larger off-nadir angles can affect the proportion of canopy returns (Holmgren et al., 2003). Fortunately, the CCLST predictor was a sufficient supplement and improved model performance in some cases. Preliminary research on the modeling of forest structure using a combination of time-

series data and LiDAR metrics has generated mixed success (Bright et al., 2017). But this study suggests the potential use of time-series derived metrics, in concert with low-density LiDAR, is worthy of further exploration.

Conclusions

This study demonstrates that low-density LiDAR can be used to provide reasonable estimates of canopy fuel attributes in the mixed forest ecosystem of northern Minnesota, USA. The results also highlight the use of pre-existing low-density LiDAR collections to complement the limited resources of forest managers to gather plot-based field data. The high-resolution map products of imputed canopy fuel attributes produced by this study improve upon the resolution and accuracy of similar products from national data repositories, such as LANDFIRE. They also potentially provide improved inputs for fire behavior models as forest managers plan for fire risk. It is encouraging that the data limitations of low-density LiDAR were generally not a major hindrance to model accuracy. These results indicate the expanded utility of low-density LiDAR and suggest re-evaluations of datasets where vegetation mapping has not yet been tested.

FINAL CONCLUSIONS

The direct measurement of forest attributes in the field is an expensive, time-consuming, and logistically difficult task. Fortunately, remote sensing and geospatial data can be used to spatially extend limited forest survey information by predicting forest attributes across unsampled areas. The results of this thesis research demonstrate two distinct applications of remote sensing and geospatial data designed to aid and enhance forest management needs at local extents.

In the first chapter, forest survey information from FIA was combined with variety of predictors from remote sensing and geospatial data to accurately classify forest stands dominated by black ash in north central Minnesota, USA. The map outputs from this study provide a new geospatial resource to forest managers in the region that can be used in concert with data and expert knowledge of hydrology, vegetation, and wildlife to anticipate local ecosystem impacts from the effects of rapid stand mortality due to EAB. In the future, the downsampled randomForest classification model methodology could be applied to other ash species to aid and enhance EAB invasion model development and regional risk assessments.

In the second chapter, a suite of metrics from low-density LiDAR (0.44 pts/m^2) were used to model five canopy fuel attributes in the mixed forest ecosystem of northeastern Minnesota, USA. To date, few studies have evaluated the accuracy of low-density LiDAR to model canopy fuel attributes. The results from this study indicate potentially unrealized, cost-efficient benefits to other low-density LiDAR collections that cover over 5,000,000 km^2 in the United States (Dept. of Commerce, 2018). The results also support previous research (Jakubowski, et al., 2013; Thomas et al., 2006; Treitz et al., 2012) suggesting that agencies and researchers should reassess

guidelines and recommendations (i.e. Mitchell et al., 2018) that advise against the use of low-density LiDAR for plot-level measurement and mapping of forest attributes.

REFERENCES

Andersen, H. E., McGaughey, R. J., & Reutebuch, S. E. (2005). Estimating forest canopy fuel parameters using LIDAR data. *Remote Sensing of Environment*, 94(4), 441–449. http://doi.org/10.1016/j.rse.2004.10.013

Anderson, R. S., & Bolstad, P. V. (2013). Estimating aboveground biomass and average annual wood biomass increment with airborne leaf-on and leaf-off LiDAR in Great Lakes Forest types. *Northern Journal of Applied Forestry*, *30*(1), 16–22. http://doi.org/10.5849/njaf.12-015

Boudreau, J., Nelson, R. F., Margolis, H. A., Beaudoin, A., Guindon, L., & Kimes, D. S. (2008). Regional aboveground forest biomass using airborne and spaceborne LiDAR in Québec. *Remote Sensing of Environment*, *112*(10), 3876–3890. http://doi.org/10.1016/j.rse.2008.06.003

Cafri, G., & Bailey, B. A. (2016). Understanding Variable Effects from Black Box Prediction: Quantifying Effects in Tree Ensembles Using Partial Dependence. *Journal of Data Science*, *14*, 67–96. http://www.jds-online.com/volume-14-number-1-january-2016

Crookston, Nicholas L.; Finley, Andrew O. 2007. yaImpute: An R Package for k-NN Imputation. Journal of Statistical Software. 23(10):1-16. *Journal of Statistical Software*, *23*(10), 1–16. http://doi.org/10.18637/jss.v023.i10

Cruz, M. G., Alexander, M. E., & Wakimoto, R. H. (2003). Assessing canopy fuel stratum characteristics in crown fire prone fuel types of western North America. *International Journal of Wildland Fire*, *12*(1), 39. http://doi.org/10.1071/WF02024

Cutler, D. R., Edwards, T. C., Beard, K. H., Cutler, A., Hess, K. T., Gibson, J., & Lawler, J. J. (2007). Random forests for classification in ecology. *Ecology*, *88*(11), 2783–2792. http://doi.org/10.1890/07-0539.1

Department of Commerce (DOC), National Oceanic and Atmospheric Administration (NOAA), National Ocean Service (NOS), Office for Coastal Management (OCM) (2018). *United States Interagency Elevation Inventory (USIEI) Viewer - Topographic/Bathymetric Data, March 2018.* NOAA's Ocean Service, Office for Coastal Management (OCM). Charleston, SC. Available at: https://coast.noaa.gov/inventory

Erdody, T. L., & Moskal, L. M. (2010). Fusion of LiDAR and imagery for estimating forest canopy fuels. *Remote Sensing of Environment*, *114*(4), 725–737. http://doi.org/10.1016/j.rse.2009.11.002

Erni, S., Arseneault, D., & Parisien, M.-A. (2018). Stand Age Influence on Potential Wildfire Ignition and Spread in the Boreal Forest of Northeastern Canada. *Ecosystems*, 1–16. https://doi.org/10.1007/s10021-018-0235-3

Eskelson, B. N. I., Barrett, T. M., & Temesgen, H. (2009). Imputing mean annual change to estimate current forest attributes. *Silva Fennica*, *43*(4), 649–658. http://doi.org/doi:10.14214/sf.185

Evans J.S. and Murphy M.A. (2017). *rfUtilities*. R package version 2.1-2, https://cran.r-project.org/package=rfUtilities.

Evans, J. S., Murphy, M. A., Holden, Z. A., & Cushman, S. A. (2011). Modeling Species Distribution and Change Using Random Forest. In *Predictive Species and Habitat Modeling in Landscape Ecology* (Vol. 86, pp. 139–159). New York, NY: Springer New York. http://doi.org/10.1007/978-1-4419-7390-0_8

Falkowski, M. J., Evans, J. S., Martinuzzi, S., Gessler, P. E., & Hudak, A. T. (2009). Characterizing forest succession with lidar data: An evaluation for the Inland Northwest, USA. *Remote Sensing of Environment*, *113*(5), 946–956. http://doi.org/10.1016/j.rse.2009.01.003

Falkowski, M. J., Hudak, A. T., Crookston, N. L., Gessler, P. E., Uebler, E. H., & Smith, A. M. S. (2010). Landscape-scale parameterization of a tree-level forest growth model: a k- nearest neighbor imputation approach incorporating LiDAR data. *Canadian Journal of Forest Research*, *40*(2), 184–199. http://doi.org/10.1139/X09-183

Fekety, P. A., Falkowski, M. J., & Hudak, A. T. (2015). Temporal transferability of LiDAR-based imputation of forest inventory attributes. *Canadian Journal of Forest Research*, 45(4), 422–435. http://doi.org/10.1139/cjfr-2014-0405

Finney, M. A. (2004). *FARSITE: Fire Area Simulator-model development and evaluation*. Research Paper RMRS-RP-4 Revised. Ogden, UT: U.S. Department of Agriculture, Forest Service, Rocky Mountain Research Station. https://doi.org/10.2737/RMRS-RP-4

Finney, M. A. (2006). An overview of FlamMap fire modeling capabilities. In: Fuels management—how to measure success: conference proceedings. 2006 March 28-30; Portland, Oregon. *Proceedings RMRS-P-41*. Fort Collins, CO: U.S. Department of Agriculture, Forest Service, Rocky Mountain Research Station: 213-220.

Flannigan, M., Stocks, B., & Wotton, B. (2000). Climate change and forest fires. *Science of The Total Environment*, *262*(3), 221–229. http://doi.org/10.1016/S0048-9697(00)00524-6

Franco-Lopez, H., Ek, A. R., & Bauer, M. E. (2001). Estimation and mapping of forest stand density, volume, and cover type using the k-nearest neighbors method. *Remote Sensing of Environment*, *77*(3), 251–274. https://doi.org/10.1016/S0034-4257(01)00209-7

González-Ferreiro, E., Diéguez-Aranda, U., Crecente-Campo, F., Barreiro-Fernández, L., Miranda, D., & Castedo-Dorado, F. (2014). Modelling canopy fuel variables for Pinus radiata D. Don in NW Spain with low-density LiDAR data. *International Journal of Wildland Fire*, *23*(3), 350. http://doi.org/10.1071/WF13054

González-Ferreiro, E., Arellano-Pérez, S., Castedo-Dorado, F., Hevia, A., Antonio Vega, J., Vega-Nieva, D., … Ruiz-González, A. D. (2017). Modelling the vertical distribution of canopy fuel load using national forest inventory and low-density airbone laser scanning data. *PLoS ONE*, *12*(4), e0176114. http://doi.org/10.1371/journal.pone.0176114

González-Olabarria, J.-R., Rodríguez, F., Fernández-Landa, A., & Mola-Yudego, B. (2012). Mapping fire risk in the Model Forest of Urbión (Spain) based on airborne LiDAR measurements. Forest Ecology and Management, 282, 149–156. http://doi.org/10.1016/j.foreco.2012.06.056

Government Accounting Office (GAO). (2017). Wildland Fire Risk Reduction: Multiple Factors Affect Federal-Nonfederal Collaboration, but Action Could Be Taken to Better Measure Progress GAO-17-357: Published: May 10, 2017. Available from: https://www.gao.gov/products/GAO-17-357. Accessed on February 9, 2018.

Hall, S. A., Burke, I. C., Box, D. O., Kaufmann, M. R., & Stoker, J. M. (2005). Estimating stand structure using discrete-return lidar: An example from low density, fire prone ponderosa pine forests. Forest Ecology and Management, 208(1–3), 189–209. http://doi.org/10.1016/j.foreco.2004.12.001

Hawbaker, T. J., Gobakken, T., Lesak, A., Trømborg, E., & Contrucci, K. (2010). Light Detection and Ranging-Based Measures of Mixed Hardwood Forest Structure. *Forest Science*, *56*(3), 313–326. Retrieved from http://www.ingentaconnect.com/content/saf/fs/2010/00000056/00000003/art00008#

Hayashi, R., Weiskittel, A., & Sader, S. (2014). Assessing the feasibility of low-density LiDAR for stand inventory attribute predictions in complex and managed forests of Northern Maine, USA. *Forests*, *5*(2), 363–383. http://doi.org/10.3390/f5020363

Heinselman, M. L. (1973). Fire in the virgin forests of the Boundary Waters Canoe Area, Minnesota. *Quaternary Research*, 3(3), 329–382. http://doi.org/10.1016/0033-5894(73)90003-3

Heinselman, M. L. (1996). *The boundary waters wilderness ecosystem*. University of Minnesota Press.

Hermosilla, T., Ruiz, L. A., Kazakova, A. N., Coops, N. C., & Moskal, L. M. (2014). Estimation of forest structure and canopy fuel parameters from small-footprint full-waveform LiDAR data. *International Journal of Wildland Fire*, *23*(2), 224–233. http://doi.org/10.1071/WF13086

Holmgren, J., Nilsson, M., & Olsson, H. (2003). Simulating the effects of lidar scanning angle for estimation of mean tree height and canopy closure. *Canadian Journal of Remote Sensing*, *29*(5), 623–632. https://doi.org/10.5589/m03-030

Hoover, C. M., Ducey, M. J., Colter, R. A., & Yamasaki, M. (2018). Evaluation of alternative approaches for landscape-scale biomass estimation in a mixed-species northern forest. *Forest Ecology and Management*, *409*(November 2017), 552–563. http://doi.org/10.1016/j.foreco.2017.11.040

Hosking, J. R. M. (1990). L-moments: Analysis and estimation of distributions using linear combinations of order statistics. *Royal Statistical Society*, *52*(1), 105–124. http://doi.wiley.com/10.1002/9781118445112.stat00570.pub2

Hudak, A. T., Crookston, N. L., Evans, J. S., Falkowski, M. J., Smith, A. M. S., Gessler, P. E., & Morgan, P. (2006). Regression modeling and mapping of coniferous forest basal area and tree density from discrete-return lidar and multispectral satellite data. *Canadian Journal of Remote Sensing*, *32*(2), 126–138. http://doi.org/10.5589/m06-007

Hudak, A. T., Crookston, N. L., Evans, J. S., Hall, D. E., & Falkowski, M. J. (2008). Nearest neighbor imputation of species-level, plot-scale forest structure attributes from LiDAR data. *Remote Sensing of Environment*, *112*(5), 2232–2245. http://doi.org/10.1016/j.rse.2007.10.009

Hudak, A. T., Tod Haren, A., Crookston, N. L., Liebermann, R. J., & Ohmann, J. L. (2014). Imputing forest structure attributes from stand inventory and remotely sensed data in western Oregon, USA. *Forest Science*, *60*(2), 253–269. http://doi.org/10.5849/forsci.12-101

Jakubowski, M. K., Guo, Q., & Kelly, M. (2013). Tradeoffs between lidar pulse density and forest measurement accuracy. *Remote Sensing of Environment*, 130, 245–253. http://doi.org/10.1016/j.rse.2012.11.024

Kalamees, R., Pussa, K., Vanha-Majamaa, I., & Zobel, K. (2005). The effects of fire and stand age on seedling establishment of Pulsatilla patens in a pine-dominated boreal forest. *Canadian Journal of Botany-Revue Canadienne De Botanique*, *83*(6), 688–693. https://doi.org/10.1139/b05-038

Kane, V. R., McGaughey, R. J., Bakker, J. D., Gersonde, R. F., Lutz, J. A., & Franklin, J. F. (2010). Comparisons between field- and LiDAR-based measures of stand structural complexity. *Canadian Journal of Forest Research*, *40*(4), 761–773. http://doi.org/10.1139/X10-024

Keane, R. E., Burgan, R., & van Wagtendonk, J. (2001). Mapping wildland fuels for fire management across multiple scales: Integrating remote sensing, GIS, and biophysical modeling. *Ecological Applications*, *14*(4), 301. http://doi.org/10.1890/02-5145

Keane, R. E., Ryan, K. C., Veblen, T. T., Allen, C. D., Logan, J., & Hawkes, B. (2002). *Cascading effects of fire exclusion in the Rocky Mountain ecosystems: a literature review*. *General Technical Report. RMRS- GTR-91*. http://doi.org/10.2737/RMRS-GTR-91

Keane, R. E., Reinhardt, E. D., Scott, J., Gray, K., & Reardon, J. (2005). Estimating forest canopy bulk density using six indirect methods. *Canadian Journal of Forest Research*, *35*(3), 724–739. http://doi.org/10.1139/x04-213

King, D. (1990). The Adaptive Significance of Tree Height. *The American Naturalist*, 135(6), 809-828. Retrieved from http://www.jstor.org/stable/2462315

Krasnow, K., Schoennagel, T., & Veblen, T. T. (2009). Forest fuel mapping and evaluation of LANDFIRE fuel maps in Boulder County, Colorado, USA. *Forest Ecology and Management*, *257*(7), 1603–1612. http://doi.org/10.1016/j.foreco.2009.01.020

LANDFIRE (2001a). LANDFIRE National Eastern Milestone Overall Quality Assessment Report https://www.landfire.gov/documents/LANDFIRENationalEasternAgreementAssessmentSummary.pdf

LANDFIRE (2001b). LANDFIRE Product Assessment: Eastern Milestone Super Zone Analysis and Report. https://www.landfire.gov/downloadfile.php?file=LANDFIRENationalEasternAgreementAssessmentSuperZoneAnalysis.pdf

Latifi, H., & Koch, B. (2012). Evaluation of most similar neighbour and random forest methods for imputing forest inventory variables using data from target and auxiliary stands. *International Journal of Remote Sensing*, *33*(21), 6668–6694. http://doi.org/10.1080/01431161.2012.693969

Latifi, H., Nothdurft, A., & Koch, B. (2010). Non-parametric prediction and mapping of standing timber volume and biomass in a temperate forest: application of multiple optical/LiDAR-derived predictors. *Forestry*, *83*(4), 395–407. http://doi.org/10.1093/forestry/cpq022

Lefsky, M. A., Harding, D., Cohen, W. B., Parker, G., & Shugart, H. H. (1999). Surface lidar remote sensing of basal area and biomass in deciduous forests of eastern Maryland, USA. *Remote Sensing of Environment*, *67*(1), 83–98. http://doi.org/10.1016/S0034-4257(98)00071-6

Lefsky, M. A., Cohen, W. B., & Spies, T. A. (2001). An evaluation of alternate remote sensing products for forest inventory, monitoring, and mapping of Douglas-fir forests in western Oregon. *Canadian Journal of Forest Research*, *31*(1), 78–87. http://doi.org/10.1139/x00-142

Lefsky, M. A., Cohen, W. B., Parker, G. G., & Harding, D. J. (2002). Lidar Remote Sensing for Ecosystem Studies. *BioScience*, *52*(1), 19. http://doi.org/10.1641/0006-3568(2002)052[0019:LRSFES]2.0.CO;2

Li, M., Im, J., Quackenbush, L. J., & Liu, T. (2014). Forest Biomass and Carbon Stock Quantification Using Airborne LiDAR Data: A Case Study Over Huntington Wildlife Forest in the Adirondack Park. *IEEE Journal of Selected Topics in Applied Earth Observations and Remote Sensing*, *7*(7), 3143–3156. http://doi.org/10.1109/JSTARS.2014.2304642

Liaw, A., & Wiener, M. (2002). Classification and Regression by randomForest. *R News*, *2* (December), 18–22. https://doi.org/10.1177/154405910408300516

Lim, K., Treitz, P., Wulder, M., St-Onge, B., & Flood, M. (2003). LiDAR remote sensing of forest structure. *Progress in Physical Geography*, *27*(1), 88–106. https://doi.org/10.1191/0309133303pp360ra

Lim, K., Hopkinson, C., & Treitz, P. (2008). Examining the effects of sampling point densities on laser canopy height and density metrics. *Forestry Chronicle*, *84*(6), 876–885. http://doi.org/10.5558/tfc84876-6

Littell, J. S., Peterson, D. L., Riley, K. L., Liu, Y., & Luce, C. H. (2016). A review of the relationships between drought and forest fire in the United States. *Global Change Biology*, *22*(7), 2353–2369. https://doi.org/10.1111/gcb.13275

Maguya, A. S., Tegel, K., Junttila, V., Kauranne, T., Korhonen, M., Burns, J., … Sanz, B. (2015). Moving Voxel Method for Estimating Canopy Base Height from Airborne Laser Scanner Data. *Remote Sensing*, *7*(7), 8950–8972. http://doi.org/10.3390/rs7078950

McGaughey, R. J. (2012). FUSION/LDV: software for LIDAR data analysis and visualization. USDA Forest Service. Pacific Northwest Research Station. Available from: http://forsys.sefs.uw.edu/fusion/fusionlatest.html

Mitchell, B., Fisk, H., Clark, J., Rounds, E. (2018). Lidar Acquisition Specifications for Forestry Applications. *USDA National Lidar Strategy.* Geospatial Technology & Applications Center. Salt Lake City, UT. https://www.fs.fed.us/eng/rsac/lidar_training/pdf/Lidar_Acquisition_Specifications.pdf Accessed 6/19/2018.

MNGEO. (2017). *LiDAR Elevation, Arrowhead Region, NE Minnesota*. Minnesota Geospatial Information Office: Minnesota Department of Natural Resources. Available from: http://www.mngeo.state.mn.us/chouse/metadata/lidar_arrowhead2011.html Accessed December 17, 2017.

Montagnoli, A., Fusco, S., Terzaghi, M., Kirschbaum, A., Pflugmacher, D., Cohen, W. B., … Chiatante, D. (2015). Estimating forest aboveground biomass by low density lidar data in mixed broad-leaved forests in the Italian Pre-Alps. *Forest Ecosystems*, *2*(1), 10. http://doi.org/10.1186/s40663-015-0035-6

Murphy, M. A., Evans, J. S., & Storfer, A. (2010). Quantifying Bufo boreas connectivity in Yellowstone National Park with landscape genetics. *Ecology*, *91*(1), 252–261. http://doi.org/10.1890/08-0879.1

National Interagency Fire Center (NIFC). (2018). *Federal Firefighting Costs (Suppression Only)*. Available from: https://www.nifc.gov/fireInfo/fireInfo_documents/SuppCosts.pdf Accessed February 7, 2018.

Packalén, P., Temesgen, H., & Maltamo, M. (2012). Variable selection strategies for nearest neighbor imputation methods used in remote sensing based forest inventory. *Canadian Journal of Remote Sensing*, *38*(5), 557–569. http://doi.org/10.5589/m12-046

Perala, D. A., Alban, D. (1993). Allometric biomass estimators for aspen-dominated ecosystems in the upper Great Lakes. *Research Paper NC-314*. St. Paul, MN: U.S. Dept. of Agriculture, Forest Service, North Central Forest Experiment Station https://doi.org/10.2737/NC-RP-314

Pierce, A. D., Farris, C. A., & Taylor, A. H. (2012). Use of random forests for modeling and mapping forest canopy fuels for fire behavior analysis in Lassen Volcanic National Park, California, USA. *Forest Ecology and Management*, *279*, 77–89. https://doi.org/10.1016/j.foreco.2012.05.010

Popescu, S. C., & Zhao, K. (2008). A voxel-based lidar method for estimating crown base height for deciduous and pine trees. *Remote Sensing of Environment*, *112*(3), 767–781. http://doi.org/10.1016/j.rse.2007.06.011

Powell, S. L., Cohen, W. B., Healey, S. P., Kennedy, R. E., Moisen, G. G., Pierce, K. B., & Ohmann, J. L. (2010). Quantification of live aboveground forest biomass dynamics with Landsat time-series and field inventory data: A comparison of empirical modeling approaches. *Remote Sensing of Environment*, 114(5), 1053–1068. https://doi.org/10.1016/j.rse.2009.12.018

Racine, E. B., Coops, N. C., St-Onge, B., & Begin, J. (2014). Estimating forest stand age from LiDAR-derived predictors and nearest neighbor imputation. *Forest Science*, *60*(1), 128–136. http://doi.org/10.5849/forsci.12-088

Reutebuch, S. E., Andersen, H. E., & McGaughey, R. J. (2005). Light detection and ranging (LIDAR): an emerging tool for multiple resource inventory. *Journal of Forestry*, *103*(6), 286-292. https://doi.org/10.1093/jof/103.6.286

Riaño, D., Valladares, F., Condés, S., & Chuvieco, E. (2004a). Estimation of leaf area index and covered ground from airborne laser scanner (Lidar) in two contrasting forests. *Agricultural and Forest Meteorology*, *124*(3–4), 269–275. http://doi.org/10.1016/j.agrformet.2004.02.005

Riaño, D., Chuvieco, E., Condés, S., González-Matesanz, J., & Ustin, S. L. (2004b). Generation of crown bulk density for Pinus sylvestris L. from lidar. *Remote Sensing of Environment*, *92*(3), 345–352. http://doi.org/10.1016/j.rse.2003.12.014

Rollins, M. G. (2009). LANDFIRE: a nationally consistent vegetation, wildland fire, and fuel assessment. *International Journal of Wildland Fire*, *18*(3), 235. http://doi.org/10.1071/WF08088

Scott, J. H., & Reinhardt, E. D. (2001). *Assessing crown fire potential by linking models of surface and crown fire behavior*. Res. Pap. RMRS-RP-29. Fort Collins, CO: U.S. Department of

Agriculture, Forest Service, Rocky Mountain Research Station. 59p. http://doi.org/10.2737/RMRS-RP-29

Shendryk, I., Hellström, M., Klemedtsson, L., & Kljun, N. (2014). Low-density LiDAR and optical imagery for biomass estimation over boreal forest in Sweden. *Forests*, *5*(5), 992–1010. http://doi.org/10.3390/f5050992

Skowronski, N., Clark, K., Nelson, R., Hom, J., & Patterson, M. (2007). Remotely sensed measurements of forest structure and fuel loads in the Pinelands of New Jersey. *Remote Sensing of Environment*, *108*(2), 123–129. http://doi.org/10.1016/j.rse.2006.09.032

Stephens, S. L., & Ruth, L. W. (2005). Federal forest-fire policy in the United States. *Ecological Applications*, 15(2), 532–542. https://doi.org/10.1890/04-0545

Straub, C., & Koch, B. (2011). Enhancement of bioenergy estimations within forests using airborne laser scanning and multispectral line scanner data. *Biomass and Bioenergy*, *35*(8), 3561–3574. http://doi.org/10.1016/j.biombioe.2011.05.017

Swain, A. M. (1973). A history of fire and vegetation in northeastern Minnesota as recorded in lake sediments. *Quaternary Research*, *3*(3), 383–396. http://doi.org/10.1016/0033-5894(73)90004-5

Tang, H., Brolly, M., Zhao, F., Strahler, A. H., Schaaf, C. L., Ganguly, S., … Dubayah, R. (2014). Deriving and validating Leaf Area Index (LAI) at multiple spatial scales through lidar remote sensing: A case study in Sierra National Forest, CA. *Remote Sensing of Environment*, *143*, 131–141. http://doi.org/10.1016/j.rse.2013.12.007

Taylor, C., McCarthy, M. A., & Lindenmayer, D. B. (2014). Nonlinear Effects of Stand Age on Fire Severity. *Conservation Letters*, *7*(4), 355–370. http://doi.org/10.1111/conl.12122

Thomas, V., Treitz, P., McCaughey, J. H., & Morrison, I. (2006). Mapping stand-level forest biophysical variables for a mixedwood boreal forest using lidar: an examination of scanning density. *Canadian Journal of Forest Research*, *36*(1), 34–47. https://doi.org/10.1139/x05-230

Tiribelli, F., Kitzberger, T., & Morales, J. M. (2018). Changes in vegetation structure and fuel characteristics along post-fire succession promote alternative stable states and positive fire-vegetation feedbacks. *Journal of Vegetation Science*, (September 2017). https://doi.org/10.1111/jvs.12620

Treitz, P., Lim, K., Woods, M., Pitt, D., Nesbitt, D., & Etheridge, D. (2012). LiDAR Sampling Density for Forest Resource Inventories in Ontario, Canada. *Remote Sensing*, *4*(12), 830–848. http://doi.org/10.3390/rs4040830

United States Forest Service (USFS). (2018). *Boundary Waters Canoe Area Wilderness Permit and Visitor Use Trends 2009-2016.* https://www.fs.usda.gov/Internet/FSE_DOCUMENTS/fseprd549672.pdf Accessed February 7, 2018

Valbuena, R., Maltamo, M., Mehtätalo, L., & Packalen, P. (2017). Key structural features of Boreal forests may be detected directly using L-moments from airborne lidar data. *Remote Sensing of Environment*, *194*, 437–446. http://doi.org/10.1016/j.rse.2016.10.024

van Mantgem, P. J., Nesmith, J. C. B., Keifer, M., Knapp, E. E., Flint, A., & Flint, L. (2013). Climatic stress increases forest fire severity across the western United States. *Ecology Letters*, *16*(9), 1151–1156. http://doi.org/10.1111/ele.12151

Van Wagner, C. E. (1977). Conditions for the start and spread of crown fire. *Canadian Journal of Forest Research*, *7*(1), 23–34. https://doi.org/10.1139/x77-004

Van Wagner, C. E. (1978). Age class distribution and the forest fire cycle. *Canadian Journal of Forest Research*, 8(2), 220–227. http://doi.org/10.1139/x78-034

Vogeler, J. C., Braaten, J. D., Slesak, R. A., & Falkowski, M. J. (2018). Extracting the full value of the Landsat archive: Inter-sensor harmonization for the mapping of Minnesota forest canopy cover (1973–2015). *Remote Sensing of Environment*, 209(January), 363–374. http://doi.org/10.1016/j.rse.2018.02.046

Wagner, W., Hollaus, M., Briese, C., & Ducic, V. (2008). 3D vegetation mapping using small-footprint full-waveform airborne laser scanners. *International Journal of Remote Sensing*, *29*(5), 1433–1452. http://doi.org/10.1080/01431160701736398

Wasser, L., Day, R., Chasmer, L., & Taylor, A. (2013). Influence of Vegetation Structure on Lidar-derived Canopy Height and Fractional Cover in Forested Riparian Buffers During Leaf-Off and Leaf-On Conditions. *PLoS ONE*, *8*(1), e54776. http://doi.org/10.1371/journal.pone.0054776

Westerling, A. L. (2016). Increasing western US forest wildfire activity: sensitivity to changes in the timing of spring. *Philosophical Transactions of the Royal Society B: Biological Sciences*, *371*(1696), 20150178. https://doi.org/10.1098/rstb.2015.0178

Westerling, A. L., Hidalgo, H. G., Cayan, D. R., & Swetnam, T. W. (2006). Warming and earlier spring increase Western U.S. forest wildfire activity. *Science*, *313*(5789), 940–943. http://doi.org/10.1126/science.1128834

White, J. C., Arnett, J. T. T. R., Wulder, M. A., Tompalski, P., & Coops, N. C. (2015). Evaluating the impact of leaf-on and leaf-off airborne laser scanning data on the estimation of forest inventory attributes with the area-based approach. *Canadian Journal of Forest Research*, *45*(11), 1498–1513. http://doi.org/10.1139/cjfr-2015-0192

Wilkes, P., Jones, S. D., Suarez, L., Haywood, A., Woodgate, W., Soto-Berelov, M., … Skidmore, A. K. (2015). Understanding the Effects of ALS Pulse Density for Metric Retrieval across Diverse Forest Types. *Photogrammetric Engineering & Remote Sensing*, *81*(8), 625–635. http://doi.org/10.14358/PERS.81.8.625

Wood, J. W., Cohen, B. S., Prebyl, T. J., Conner, L. M., Collier, B. A., & Chamberlain, M. J. (2018). Time-since-fire and stand seral stage affect habitat selection of eastern wild turkeys in a managed longleaf pine ecosystem. *Forest Ecology and Management*, *411*(October 2017), 203–212. https://doi.org/10.1016/j.foreco.2018.01.033

Woods, M., Lim, K., & Treitz, P. (2008). Predicting forest stand variables from LiDAR data in the Great Lakes - St. Lawrence forest of Ontario. *The Forestry Chronicle*, *84*(6), 827–839. http://doi.org/10.5558/tfc84827-6

Zhao, K., Popescu, S., & Nelson, R. (2009). Lidar remote sensing of forest biomass: A scale-invariant estimation approach using airborne lasers. *Remote Sensing of Environment*, *113*(1), 182–196. http://doi.org/10.1016/j.rse.2008.09.009

Zhao, K., Popescu, S., Meng, X., Pang, Y., & Agca, M. (2011). Characterizing forest canopy structure with lidar composite metrics and machine learning. *Remote Sensing of Environment*, *115*(8), 1978–1996. http://doi.org/10.1016/j.rse.2011.04.001

Zheng, D., Heath, L. S., & Ducey, M. J. (2008). Spatial distribution of forest aboveground biomass estimated from remote sensing and forest inventory data in New England, USA. *Journal of Applied Remote Sensing*, *2*(1), 21502. http://doi.org/10.1117/1.2940686